Cell

ALDH7A1 protects against ferroptosis by generating membrane NADH and regulating FSP1

Graphical abstract

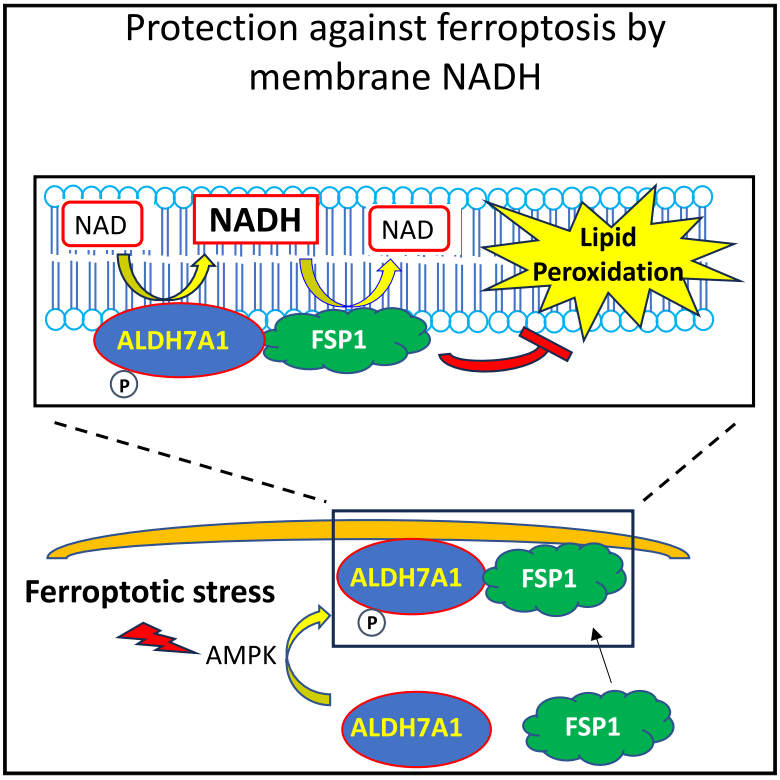

Highlights

- NADH exists at significant levels on cellular membranes
- Membrane NADH is generated by ALDH7A1 and supports FSP1 activity
- ALDH7A1 recruits FSP1 to membranes through ferroptosis-induced signaling
- ALDH7A1 also decreases lipid peroxidation by consuming reactive aldehydes

Authors

Jia-Shu Yang, Andrew J. Morris, Koki Kamizaki, ..., Marcus Conrad, Whitney S. Henry, Victor W. Hsu

Correspondence

jyang1@bwh.harvard.edu (J.-S.Y.), vhsu@bwh.harvard.edu (V.W.H.)

In brief

A membrane-associated pool of NADH confers protection against ferroptosis.

Yang et al., 2025, Cell *188*, 2569–2585
May 15, 2025
https://doi.org/10.1016/j.cell.2025.03.019

CellPress

Cell

CellPress

Article

ALDH7A1 protects against ferroptosis by generating membrane NADH and regulating FSP1

Jia-Shu Yang,[1,*] Andrew J. Morris,[2,3] Koki Kamizaki,[4] Jianzhong Chen,[2] Jillian Stark,[5] William M. Oldham,[6] Toshitaka Nakamura,[7] Eikan Mishima,[7] Joseph Loscalzo,[8] Yasuhiro Minami,[4] Marcus Conrad,[7] Whitney S. Henry,[5] and Victor W. Hsu[1,9,*]

[1]Division of Rheumatology, Inflammation and Immunity, Department of Medicine, Brigham and Women's Hospital and Harvard Medical School, Boston, MA 02115, USA

[2]Division of Cardiovascular Medicine, Department of Medicine, University of Kentucky and Lexington Veterans Affairs Medical Center, Lexington, KY 40536, USA

[3]Central Arkansas VA Healthcare System and Arkansas Children's Nutrition Research Center, University of Arkansas for Medical Sciences, Little Rock, AR 72205, USA

[4]Department of Physiology and Cell Biology, Kobe University School of Medicine, Kobe 650-0017, Japan

[5]Department of Biology, Massachusetts Institute of Technology, and Koch Institute for Integrative Cancer Research, Cambridge, MA 02139, USA

[6]Division of Pulmonary and Critical Care Medicine, Department of Medicine, Brigham and Women's Hospital and Harvard Medical School, Boston, MA 02115, USA

[7]Institute of Metabolism and Cell Death, Molecular Targets and Therapeutics Center, Helmholtz Munich, Neuherberg, Germany

[8]Cardiovascular Division, Department of Medicine, Brigham and Women's Hospital and Harvard Medical School, Boston, MA 02115, USA

[9]Lead contact

*Correspondence: jyang1@bwh.harvard.edu (J.-S.Y.), vhsu@bwh.harvard.edu (V.W.H.)

https://doi.org/10.1016/j.cell.2025.03.019

SUMMARY

Ferroptosis is a form of cell death due to iron-induced lipid peroxidation. Ferroptosis suppressor protein 1 (FSP1) protects against this death by generating antioxidants, which requires nicotinamide adenine dinucleotide, reduced form (NADH) as a cofactor. We initially uncover that NADH exists at significant levels on cellular membranes and then find that this form of NADH is generated by aldehyde dehydrogenase 7A1 (ALDH7A1) to support FSP1 activity. ALDH7A1 activity also acts directly to decrease lipid peroxidation by consuming reactive aldehydes. Furthermore, ALDH7A1 promotes the membrane recruitment of FSP1, which is instigated by ferroptotic stress activating AMP-activated protein kinase (AMPK) to promote the membrane localization of ALDH7A1 that stabilizes FSP1 on membranes. These findings advance a fundamental understanding of NADH by revealing a previously unappreciated pool on cellular membranes, with the elucidation of its function providing a major understanding of how FSP1 acts and how an aldehyde dehydrogenase protects against ferroptosis.

INTRODUCTION

The iron-dependent generation of reactive oxygen species (ROS) induces cell death through lipid peroxidation, a process known as ferroptosis.[1] Glutathione peroxidase 4 (GPX4) was initially identified to protect against this form of cell death by reducing hydroperoxides generated during lipid peroxidation.[2,3] Subsequently, ferroptosis suppressor protein 1 (FSP1) was also identified to protect against ferroptosis by generating antioxidants through the reduction of ubiquinone to ubiquinol.[4,5] This activity of FSP1 requires nicotinamide adenine dinucleotide, reduced form (NADH) as a cofactor and FSP1 to localize to membranes,[4,5] but how these requirements are met remains to be better understood. Why cells show variable dependency on FSP1 for ferroptosis protection is also unclear.

NADH participates in a variety of cellular events by acting as a cofactor in enzymatic reactions. Well-characterized examples include its participation in glycolysis that operates in the cytosol and oxidative phosphorylation that occurs in the mitochondria.[6] The currently known roles of NADH involve its soluble form, but whether NADH exists on cellular membranes at significant levels and what purpose such a pool may serve have not been studied.

We address these outstanding questions in an unexpected manner. The family of aldehyde dehydrogenases (ALDHs) converts aldehyde groups in substrates to their corresponding carboxylates in products, which involves nicotinamide adenine

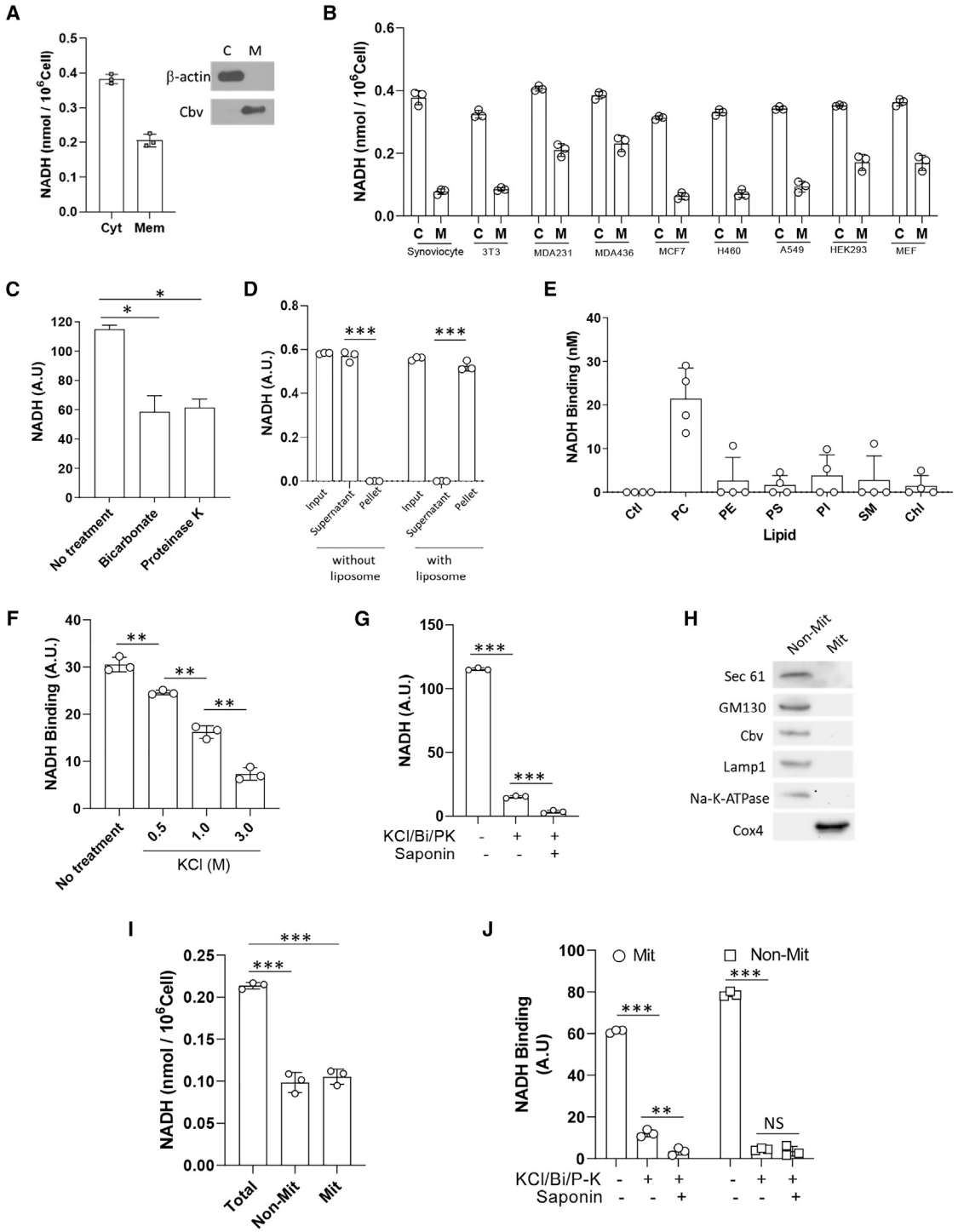

Figure 1. NADH exists at a significant level on cellular membranes

(A) NADH level in total membranes and cytosol from HeLa cells, with cellubrevin (Cbv) tracking membrane and actin tracking cytosol, $n = 3$.

(B) NADH level in total membranes (M) and cytosol (C) from different cell types as indicated, $n = 3$.

(C) Total membranes from HeLa cells were treated as indicated, and then NADH level was quantified, $n = 3$.

(D) NADH was incubated with or without liposomes, and then NADH level in the pellet and supernatant after centrifugation was quantified, $n = 3$.

(E) NADH was incubated with liposomes having different individual lipids as indicated, and then NADH level on liposomes was quantified, $n = 4$.

(F and G) Total membranes from HeLa cells were treated as indicated and then quantified for NADH level, $n = 3$.

(legend continued on next page)

dinucleotide (NAD) becoming converted to NADH. This generation of NADH is due to hydride ions being transferred from aldehydes to NAD.[7–9] Aldehyde dehydrogenase 7A1 (ALDH7A1) is a highly conserved member of this family and hence was originally named antiquitin.[10] In plants, ALDH7A1 has been suggested to protect against osmotic stress.[11] In humans, it has been identified to catalyze an intermediate step in lysine metabolism, with a defect in this role resulting in pyridoxine-dependent seizures in newborns.[12]

We recently discovered a new role for ALDH7A1, protecting against situations of cellular energy stress that include starvation and hypoxia by reducing cellular energy consumption through a broad inhibition of the intracellular transport pathways.[13] This role involves NADH generated by ALDH7A1 activity targeting key transport factors to inhibit the formation of transport carriers.[13] A curious finding is that the recruitment of soluble ALDH7A1 to membranes enhances its catalytic activity by nearly 100-fold.[13] However, because this observation is an *in vitro* finding, its physiologic significance has been unclear.

Pursuing this observation in this study, we initially uncover that NADH exists at significant levels on cellular membranes and then find that membrane NADH is controlled by ALDH7A1 activity. Further characterizations have enabled us to achieve a major understanding of how FSP1 protects against ferroptosis and also how an ALDH acts in this protection.

RESULTS

Cellular membranes contain significant levels of NADH

We previously examined HeLa cells in studying how ALDH7A1 regulates intracellular transport.[13] Thus, we initially fractionated these cells into total membranes and cytosol, which revealed a significant level of NADH on membranes (Figure 1A). As NADH has not been known to exist at such levels on cellular membranes, we next examined a variety of other cells and found that membrane NADH is a prevalent phenomenon (Figure 1B).

Native membranes contain both lipids and proteins. Thus, we next examined which of these biological components are involved in binding to NADH. Bicarbonate (Bi) wash releases peripheral proteins from membranes, while proteinase K (PK) treatment degrades proteins exposed on membrane surfaces. We found that either treatment led to about half of the membrane-bound NADH being released (Figure 1C), implying that the other half binds to lipids.

As NADH has not been expected to bind directly to lipids, we next sought to confirm this capability. Generating liposomes with a composition of major lipids that mimic those of native membranes, we found that NADH bound to these liposomes (Figure 1D). Further defining this binding, we generated liposomes having different individual lipids and found that NADH bound preferentially to phosphatidylcholine (PC) (Figure 1E).

We next considered that the choline moiety of PC is predicted to be positively charged at neutral pH. Thus, as the phosphate group of NADH is negatively charged, we explored the possibility that NADH binds to PC through electrostatic interaction by examining the effect of increasing salt concentration. Native membranes have been found to retain their integrity and function, as assessed by the reconstitution of transport vesicles, when treated with potassium chloride (KCl) up to 3M.[14,15] When the NADH-bound PC liposomes were washed with increasing KCl concentration, we observed the progressive release of NADH (Figure 1F). As PC is the predominant lipid in native membrane, we then treated total membranes with 3M KCl along with Bi and PK and found that NADH was largely displaced from total membranes (Figure 1G). However, because a residual level of NADH could still be detected on total membranes, we next considered that the mitochondria, which would be included in the total membrane fraction, contain soluble NADH in their luminal space. Thus, we examined whether the residual NADH represents this mitochondrial pool. Permeabilizing total membranes with 0.2% saponin, we found that the residual NADH was abolished (Figure 1G).

To further confirm that this residual NADH represents soluble NADH within the mitochondria, we next segregated cellular membranes into mitochondrial versus non-mitochondrial fraction (Figure 1H). Quantifying the NADH level in both fractions, we found that NADH was distributed roughly equally between the two fractions (Figure 1I). To release membrane-bound NADH in both fractions, we treated them with the combination of KCl/Bi/PK, which revealed that the residual NADH resided in the mitochondria fraction (Figure 1J). When this fraction was further subjected to 0.2% saponin treatment, the residual NADH was eliminated (Figure 1J), thus confirming that the soluble pool within the mitochondria accounts for the residual NADH.

Membrane NADH requires ALDH7A1 activity

We next treated cells with small interfering RNA (siRNA) against ALDH7A1 followed by fractionation and found that membrane NADH was preferentially decreased, with cells having higher membrane NADH level being more affected (Figure 2A). In addition, we performed clustered regularly interspaced short palindromic repeats (CRISPR)-Cas9 to knock out ALDH7A1 in HeLa cells (Figure S1A) and found that the membrane NADH level was also preferentially decreased (Figure S1B). Furthermore, the catalytic activity of ALDH7A1 was needed to support membrane NADH, as its level that was reduced by siRNA against ALDH7A1 was restored by expressing wild-type ALDH7A1 but not the catalytic-dead (E268Q) form (Figure S1C). Furthermore, siRNA against multiple other ALDH members did not reduce the membrane NADH level (Figure 2B). Thus, ALDH7A1 shows specificity in supporting the membrane NADH level.

We next examined whether ALDH7A1 controls both the protein- and lipid-bound fractions of membrane NADH. Isolating membranes that had been treated with Bi and PK to release

(H) Membrane fractions as indicated were immunoblotted for organelle markers: Sec61 (endoplasmic reticulum), GM130 (Golgi), Cbv (endosome), Lamp1 (lysosome), Na/K ATPase (plasma membrane), $n = 2$.

(I) NADH level in membrane fractions from HeLa cells was quantified, $n = 3$.

(J) Membrane fractions from HeLa cells were treated as indicated, and then NADH level was quantified, $n = 3$.

Quantitative data are shown as mean ± SD; $^{***}p < 0.0005$, $^{**}p < 0.005$, $^{*}p < 0.05$, NS $p > 0.05$, Student's t test.

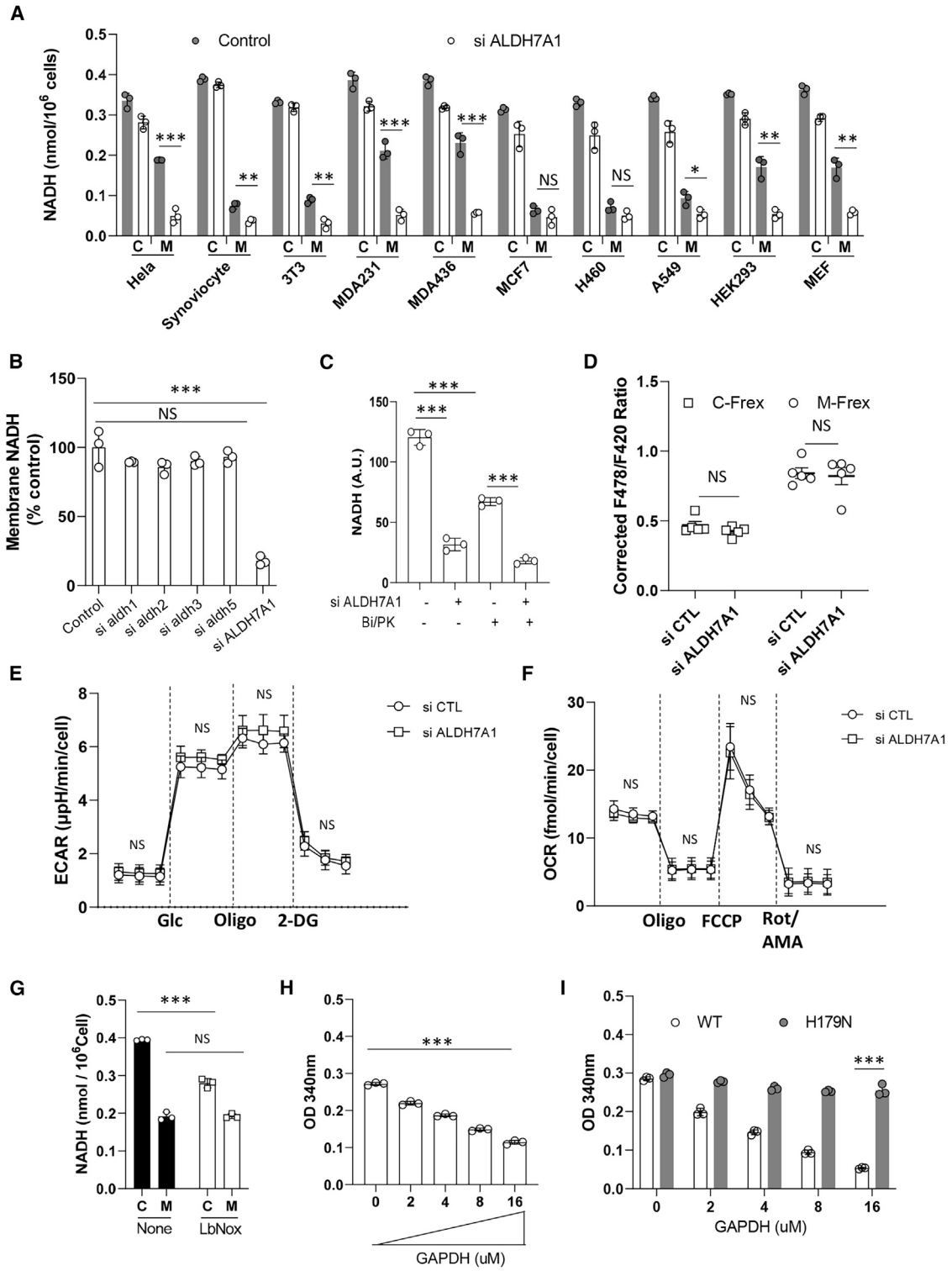

Figure 2. ALDH7A1 activity is a main determinant of membrane NADH level

(A) NADH level in total membranes and cytosol from different cell types that were treated as indicated, $n = 3$.

(B) NADH level in total membranes from HeLa cells that were treated as indicated, $n = 3$, one-way ANOVA test.

(C) Total membranes from HeLa cells were treated as indicated, and then NADH level was quantified, $n = 3$.

(D) Free NADH level in the cytosol and mitochondria of HeLa cells was quantified using biosensors as indicated, $n = 5$.

(legend continued on next page)

protein-bound NADH, we found that prior treatment with siRNA against ALDH7A1 reduced NADH levels in both total membranes and the lipid-bound fraction (Figure 2C), revealing that ALDH7A1 controls both the protein- and lipid-bound fractions of membrane NADH. We also incubated the lipid-bound fraction with buffer and found that NADH was rapidly released from the membrane before reaching a plateau (Figure S1D), revealing that NADH binds to membrane dynamically.

We next considered that the phosphorylation of ALDH7A1 at its S102 residue has been found previously to promote its membrane localization.[13] As such, we next replaced endogenous ALDH7A1 with either the S102A (which prevents phosphorylation) or S102D (which mimics phosphorylation) form. This was achieved by siRNA against ALDH7A1 followed rescue using either mutant. We found that S102A expression reduced NADH level on membranes, while S102D expression increased the membrane NADH level (Figure S1E). Thus, ALDH7A1 needs to be recruited to cellular membranes to support the membrane NADH level.

Membrane NADH acts as a distinct pool from soluble NADH in cells

We next asked whether membrane NADH behaves as a distinct pool from soluble NADH in cells. Using biosensors that have been developed to monitor free NADH level in either the cytosol or the mitochondria,[16] we found that siRNA against ALDH7A1 did not have an appreciable effect on either pool (Figure 2D). We next noted that soluble NADH has well-established roles in cellular energetics, with the cytosolic pool acting in glycolysis and the mitochondrial pool participating in oxidative phosphorylation. Upon siRNA against ALDH7A1, we found that glycolytic flux was not affected, as assessed by the extracellular acidification rate (ECAR) (Figure 2E). Mitochondrial respiration was also not affected, as assessed by the oxygen consumption rate (OCR) (Figure 2F). We also expressed an oxidase that targets only cytosolic NADH[17] and found that the membrane NADH level was not affected (Figure 2G). As the results all pointed to the soluble and membrane pools of NADH being compartmentalized, we next sought insight into how this could be achieved.

The cytosol contains many soluble proteins that bind NADH, which enables cytosolic NADH to exist in equilibrium between the free and protein-bound state. As glyceraldehyde 3-phosphate dehydrogenase (GAPDH) is one such protein, we incubated soluble NADH with liposomes and found that adding increasing levels of GAPDH led to decreasing level of NADH bound to liposomes (Figure 2H). This effect required NADH binding by GAPDH, as a mutant GAPDH that cannot bind NADH could not reduce NADH binding to liposomes (Figure 2I). Thus, these results suggested that cytosolic NADH can be compartmentalized from membrane NADH through association with cytosolic NADH-binding proteins.

Membranes also contain NADH-related compounds

As nicotinamide adenine dinucleotide phosphate reduced form (NADPH) is a derivative of NADH, we next found that NADPH also exists at significant levels on membranes in multiple cell types (Figure S1F). We also confirmed the specificity of our assays in detecting NADPH versus NADH (Figure S1G). However, in contrast to membrane NADH, siRNA against ALDH7A1 did not have an appreciable effect on the membrane NADPH level (Figure S1F), which further supported the specificity by which ALDH7A1 controls the membrane NADH level.

As ALDH7A1 activity reduces NAD to generate NADH, we next found NAD also exists at significant levels on membranes (Figure S1H). Moreover, whereas the cytosolic level of NAD did not change appreciably upon siRNA against ALDH7A1, we observed perceptible increase in the membrane NAD in some cell types (Figure S1H), which correlated with cells that have higher levels of membrane NADH (compare with Figure 2A). Thus, when also taking into consideration that membrane NAD is about 5-fold more abundant than membrane NADH, we concluded that ALDH7A1 generates membrane NADH largely by using membrane NAD.

ALDH7A1 supports FSP1 activity

We next sought to identify a function for membrane NADH. Searching the literature, we noted that FSP1 has been found to act in protection against ferroptosis, with this role involving the reduction of ubiquinone to ubiquinol, which requires NADH acting as a cofactor. Furthermore, FSP1 is only active on membranes.[4,5] Thus, we explored the possibility that membrane NADH generated by ALDH7A1 supports FSP1 activity.

As cells exhibit varying dependency on FSP1 for protection against ferroptosis,[4,5] we initially asked whether this dependency correlates with dependency on ALDH7A1. Ferroptotic stress can be induced specifically by treating cells with a sub-lethal dose (100 nM) of (1S,3R)-RSL3, RAS-selective lethal 3 (RSL3), a pharmacologic agent that inhibits GPX4 activity.[2] We found that this treatment in conjunction with siRNA against either ALDH7A1 or FSP1 led to similar magnitudes in cell death (Figure 3A) and lipid peroxidation (Figure 3B). We also confirmed the specificity of the siRNA targeting by another set of sequences, as similar levels of cell death were observed (Figure S2A). The efficacy of the siRNA treatments was also confirmed (Figure S2B). Moreover, targeting against both ALDH7A1 and FSP1 did not further increase cell death (Figure S2C) or lipid peroxidation (Figure S2D), which was consistent with ALDH7A1 and FSP1 acting in the same mechanistic pathway.

We next confirmed that the observed cell death was due to ferroptosis, as it was prevented by treatment with liproxstatin-1, ferrostatin-1, or deferoxamine, agents that protect against ferroptosis[1] but not by treatment with carbobenzoxy-valyl-alanyl-aspartyl-[O-methyl]-fluoromethylketone (zVAD-FMK) that protects

(E) ECAR in HeLa cells upon different treatments as indicated, $n = 4$.
(F) OCR in HeLa cells upon different treatments as indicated, $n = 3$.
(G) NADH level in total membranes and cytosol from HeLa cells that were treated as indicated, $n = 3$.
(H and I) Liposomes were incubated with NADH and increasing levels of GAPDH, and then NADH level on liposomes was quantified by optical density (OD) at 340 nm, $n = 3$.
Quantitative data are shown as mean ± SD; ***$p < 0.0005$, **$p < 0.005$, *$p < 0.05$, NS $p > 0.05$, Student's t test (unless indicated otherwise).
See also Figure S1.

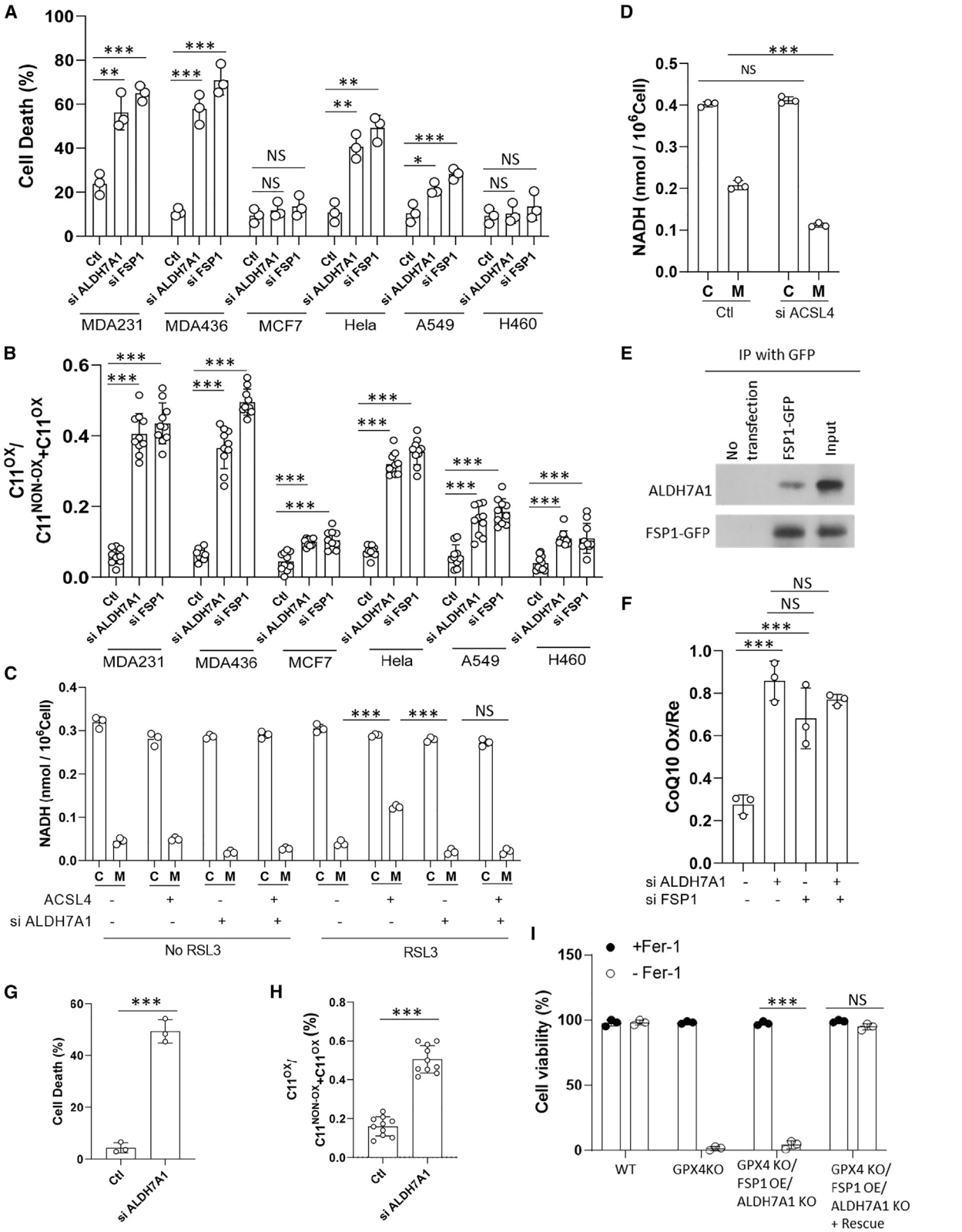

(legend on next page)

against apoptosis[18] or with Necrostatin-1 that protects against necroptosis[19] (Figure S2E). Ferroptosis can also be induced by targeting upstream components of the GPX4 mechanism, such as erastin treatment that inhibits the uptake of cystine, which is needed for the synthesis of glutathione that supports GPX4 activity.[20] We found that a sub-lethal dose of erastin (2 μM) in conjunction with siRNA against either ALDH7A1 or FSP1 also induced similar degrees of cell death (Figure S2F) and lipid peroxidation (Figure S2G).

We next explored whether a protective role by ALDH7A1 against ferroptosis also explains why cells show variable levels of membrane NADH. Lipids that contain polyunsaturated fatty acids (PUFAs) are particularly targeted for lipid peroxidation in driving ferroptosis, and acyl-coenzyme A (CoA) synthase 4 (ACSL4) has been found to act as a key enzyme in the synthesis of PUFAs.[21,22] Cells with low ACSL4 expression, such as MCF7 cells, have been shown previously to be less sensitive to ferroptosis but can be converted to become more sensitive by increasing ACSL4 expression.[21] We first confirmed that overexpressing ACSL4 in MCF7 cells through transfection (Figure S3A) led to increased sensitivity to ferroptotic stress induced by RSL3 treatment, as assessed by cell death (Figure S3B) and lipid peroxidation (Figure S3C). We then found that ACSL4 overexpression resulted in RSL3 treatment increasing the membrane NADH level more dramatically, with this increase being dependent on ALDH7A1 (Figure 3C).

We next performed the converse experiment by examining MDA231 cells, which show high sensitivity to ferroptotic stress (see Figure 3A) and have a high level of membrane NADH (see Figure 1B). For these studies, we used high-dose RSL3 treatment (1 μM) so that the effects of reducing ACSL4 level on cell death and lipid peroxidation could be better discerned. The results confirmed that siRNA against ACSL4 (Figure S3D) led to less cell death (Figure S3E) and lipid peroxidation (Figure S3F), as well as decreased membrane NADH level (Figure 3D). Thus, by revealing that membrane NADH level is responsive to the degree that cells are susceptible to ferroptosis, we have also uncovered an explanation for why cells show variable levels of membrane NADH.

We next sought more direct evidence that ALDH7A1 is needed for FSP1 activity. Performing a co-precipitation experiment, we found that ALDH7A1 interacts with FSP1 in MDA231 cells (Figure 3E) and in multiple other cell types (Figure S3G). As FSP1 converts ubiquinone to ubiquinol, we also found that siRNA against ALDH7A1 increased the ubiquinone/ubiquinol (also known as the coenzyme Q10 oxidized/reduced) ratio in cells, and the extent of this increase was similar to that induced by siRNA against FSP1 (Figure 3F). Moreover, targeting against both proteins did not further increase this ratio (Figure 3F), which further supported that ALDH7A1 and FSP1 act in the same mechanistic pathway.

We then noted that HT1080 cells, which depend mainly on GPX4 for protection against ferroptosis, have been converted to depend on FSP1 by knocking out GPX4 and overexpressing FSP1 (HT1080/GPX4 knockout [KO]/FSP1 OE).[23,24] Upon FINO2 treatment, which provides a way of inducing ferroptotic stress without directly targeting GPX4 activity,[25] we found that further treatment of these converted cells with siRNA against ALDH7A1 resulted in substantial cell death (Figure 3G) and lipid peroxidation (Figure 3H).

To further confirm the critical role that ALDH7A1 plays in these converted cells, we knocked out ALDH7A1 using CRISPR-Cas9 (Figure S3H) and found that the resulting cells (HT1080/GPX4 KO/FSP1 OE/ALDH7A1 KO) could not even survive under normal condition but instead required treatment with ferrostatin-1 (Figure 3I) or the re-expression of ALDH7A1 (Figure 3I) to survive. We also pursued animal studies and confirmed that these KO cells showed markedly reduced ability to grow as tumors in mice (Figures S3I and S3J).

Reconstituting protection against lipid peroxidation by ALDH7A1 and FSP1

We next considered that cell-based studies cannot rule out indirect effects. Thus, to confirm that ALDH7A1 activity directly supports FSP1 activity, we sought to reconstitute both activities using purified components. We first incubated ALDH7A1 and FSP1 as purified proteins to confirm that they can interact directly (Figure 4A). Next, to reconstitute ALDH7A1 activity, we generated liposomes having a composition of major lipids that mimic those of native membranes. Upon incubating these liposomes with recombinant ALDH7A1 in the presence of a model substrate (octanal) and NAD, we found that the S102D but not the S102A form reconstituted ALDH7A1 activity, as tracked by the generation of NADH (Figure 4B). As control, incubation with a catalytic-dead mutant of the S102D form did not generate NADH (Figure 4B). NADH was also not produced when either octanal or NAD was omitted from the incubation (Figure 4B). We also confirmed that the generated NADH was bound to liposomes (Figure 4C).

Next, to reconstitute FSP1 activity, we incorporated ubiquinone into liposomes and first confirmed the reconstitution of ALDH7A1 activity using these liposomes, as tracked by the generation of NADH (Figure 4D). We then added FSP1 and found that the generated NADH level was decreased (Figure 4D). As control, we found that a catalytic-dead form of FSP1

Figure 3. ALDH7A1 protects against ferroptosis through FSP1

(A) Cell death was quantified upon treatment with RSL3 (100 nM) and siRNA as indicated, $n = 3$.

(B) Lipid peroxidation was quantified upon treatment with RSL3 (100 nM) and siRNA as indicated, $n = 3$. A representative experiment is shown.

(C) NADH level in total membranes and cytosol from MCF7 cells that were treated as indicated, RSL3 (100 nM), $n = 3$.

(D) NADH level in total membranes and cytosol from MDA231 cells that were treated as indicated, $n = 3$.

(E) Interaction between endogenous ALDH7A1 and transfected GFP-tagged FSP1 in MDA231 cells as assessed by a co-precipitation experiment, $n = 2$.

(F) CoQ10 ox/red ratio in MDA231 cells that had been treated as indicated, $n = 3$.

(G and H) Cell death (G) and lipid peroxidation (H) were quantified for HT1080/GPX4 KO/FSP1 OE cells that were treated with FINO2 and siRNA as indicated, $n = 3$.

(I) Cell death was quantified for different forms of HT1080 cells with treatment as indicated, $n = 3$.

Quantitative data are shown as mean ± SD; $^{***}p < 0.0005$, $^{**}p < 0.005$, $^{*}p < 0.05$, NS $p > 0.05$, Student's t test.

See also Figures S2 and S3.

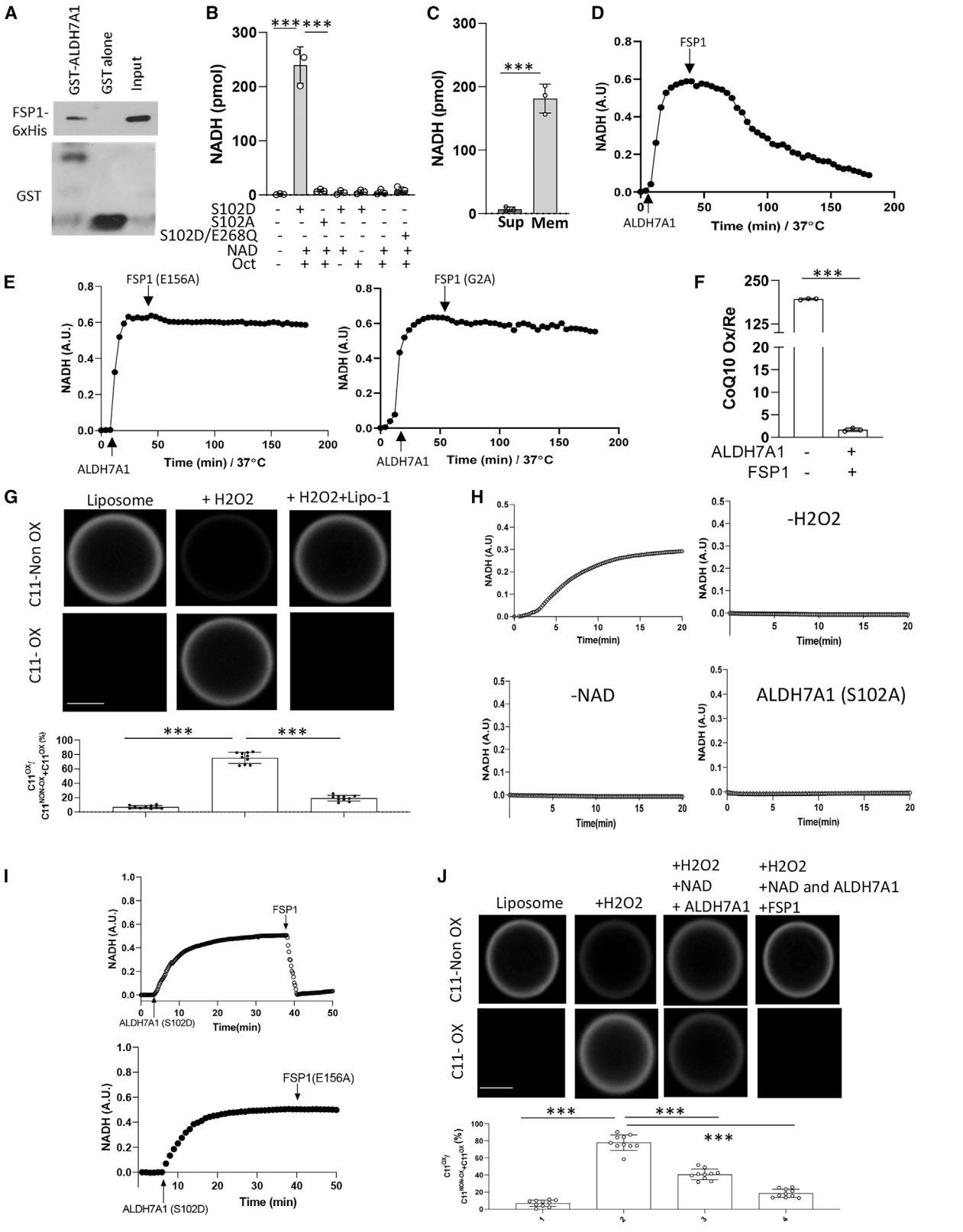

(legend on next page)

(E156A)[5,26] did not decrease the NADH level (Figure 4E). A mutant FSP1 that lacks myristoylation (G2A), which cannot be recruited to membranes,[4,5] also did not decrease the NADH level (Figure 4E). Further confirming that FSP1 activity was reconstituted, we found that ubiquinone on the liposomes was converted to ubiquinol (Figure 4F). Thus, these results provided more definitive support that membrane NADH generated by ALDH7A1 supports FSP1 activity.

Having reconstituted ALDH7A1 and FSP1 activities, we then sought to reconstitute their protection against lipid peroxidation. As phosphatidylethanolamine (PE) that contains PUFA has been identified as a key target of ferroptosis-induced lipid peroxidation,[21,22] we incorporated PUFA-PE into the liposomes. We then found that simply adding hydrogen peroxide reconstituted lipid peroxidation, as assessed by the biosensor (Figure 4G), which was further confirmed by the addition of liproxstatin-1 that suppressed the biosensor signal (Figure 4G). We then added ALDH7A1-S102D and NAD, and remarkably, without adding a substrate for ALDH7A1, we observed NADH generation (Figure 4H). As control, incubation using liposomes not treated with hydrogen peroxide did not generate NADH (Figure 4H). NADH also was not generated when NAD was not added (Figure 4H) or when the soluble form of ALDH7A1 (S102A) was used (Figure 4H). Thus, we have not only reconstituted lipid peroxidation but also revealed that lipid peroxidation generates substrates for ALDH7A1 activity.

We next sought to reconstitute FSP1 activity in this setting. After reconstituting ALDH7A1 activity using liposomes that had been subjected to lipid peroxidation, we found that the subsequent addition of FSP1 decreased the NADH level (Figure 4I). As control, the NADH level was not decreased when the catalytic-dead form of FSP1 was used (Figure 4I). We also confirmed that reconstituting FSP1 activity led to decreased lipid peroxidation, as assessed by the biosensor (Figure 4J). Further notable was that reconstituting only ALDH7A1 activity led to a partial decrease in lipid peroxidation (Figure 4J). Thus, the results revealed that ALDH7A1 protects against lipid peroxidation through two complementary mechanisms: by supporting FSP1 activity and by an FSP1-independent mechanism.

To elucidate this FSP1-independent mechanism, we were led by the consideration that ALDH7A1 converts aldehydes to carboxylates.[7,8] Thus, as lipid peroxidation generates reactive aldehydes, for which 4-hydroxynonenal (4-HNE) and malonaldehyde (MDA) are considered prototypic ones,[27] we first confirmed that our reconstitution of lipid peroxidation generated 4-HNE (Figure 5A) and MDA (Figure 5B). We then found that reconstituting ALDH7A1 activity reduced the level of both aldehydes (Figures 5A and 5B).

In principle, this reduction could be due to ALDH7A1 activity preventing the generation of these aldehydes rather than consuming them. Thus, to distinguish between these two possibilities, we added these aldehydes to liposomes that had not been subjected to lipid peroxidation. We then incubated these liposomes with the membrane-bound form of ALDH7A1 (S102D) and NAD and found that the levels of both added aldehydes were decreased (Figures 5C and 5D), confirming that ALDH7A1 reduces the levels of these aldehydes by consuming them. We also confirmed that the added aldehydes were recruited to liposomes, as NADH generation by ALDH7A1 was dependent on the S102D form (Figures 5E and 5F).

We next sought to confirm the above findings in cells. Upon siRNA against ALDH7A1, we found that both 4-HNE (Figure 5G) and MDA (Figure 5H) levels in MDA231 cells were increased, and notably, siRNA against FSP1 did not have a similar effect. We also performed rescues and found that the expression of the S102D but not the S102A form of ALDH7A1 prevented the increases (Figures 5I and 5J). Thus, these results provided cell-based support that the FSP1-independent mechanism of protection against lipid peroxidation involves ALDH7A1 activity decreasing the level of reactive aldehydes.

We next considered that hydrogen peroxide is a relatively weak inducer of lipid peroxidation. Thus, we examined whether the use of (E)-1,2-bis((2-methyldecan-2-yl)oxy)diazen (DTUN), which is a stronger inducer of lipid peroxidation,[28] would lead to similar results. We first confirmed that lipid peroxidation of liposomes was similarly reconstituted upon adding DTUN, as assessed by the biosensor, which was further confirmed by the addition of liproxstatin-1 that suppressed the biosensor signal (Figure S4A). Moreover, the addition of ALDH7A1 decreased

Figure 4. Reconstituting protection against lipid peroxidation by ALDH7A1 and FSP1

(A) Direct interaction between ALDH7A1 and FSP1 was assessed by a pull-down experiment using purified components, $n = 2$.

(B) Liposomes were incubated with NAD, octanal, and ALDH7A1 form as indicated, and then NADH level on liposomes was quantified, $n = 3$.

(C) Liposomes were incubated with NAD, octanal, and ALDH7A1 form as indicated, and then the levels of liposome-bound NADH and soluble NADH were quantified, $n = 3$.

(D and E) NADH level, as tracked by OD at 340 nm, was quantified upon reconstituting ALDH7A1 activity (by incubating liposomes with NAD, octanal, and ALDH7A1) and upon the further addition of FSP1 forms as indicated, $n = 3$.

(F) CoQ10 ox/red ratio comparing when both ALDH7A1 and FSP1 activities were reconstituted versus when neither activity was reconstituted, $n = 3$.

(G) Lipid peroxidation of liposomes in different conditions as indicated was assessed by confocal microscopy detecting the biosensor, $n = 3$. A representative experiment is shown having primary images, bar: 10 μm, and quantitation.

(H) NADH level, as tracked by OD at 340 nm, was quantified, comparing when ALDH7A1 activity was reconstituted (by incubating liposomes subjected to hydrogen peroxide with NAD and ALDH7A1) versus conditions when different components are omitted or when mutant ALDH7A1 was used, $n = 3$.

(I) NADH level, as tracked by OD at 340 nm, was quantified upon reconstituting ALDH7A1 activity (by incubating liposomes that had been exposed to hydrogen peroxide with NAD and ALDH7A1) and upon the further addition of FSP1 forms as indicated, $n = 3$.

(J) Lipid peroxidation of liposomes in different conditions as indicated was assessed by confocal microscopy detecting the biosensor, $n = 3$. A representative experiment is shown having primary images, bar: 10 μm, and quantitation.

Quantitative data are shown as mean ± SD; $^{***}p < 0.0005$, Student's t test.

See also Figure S4.

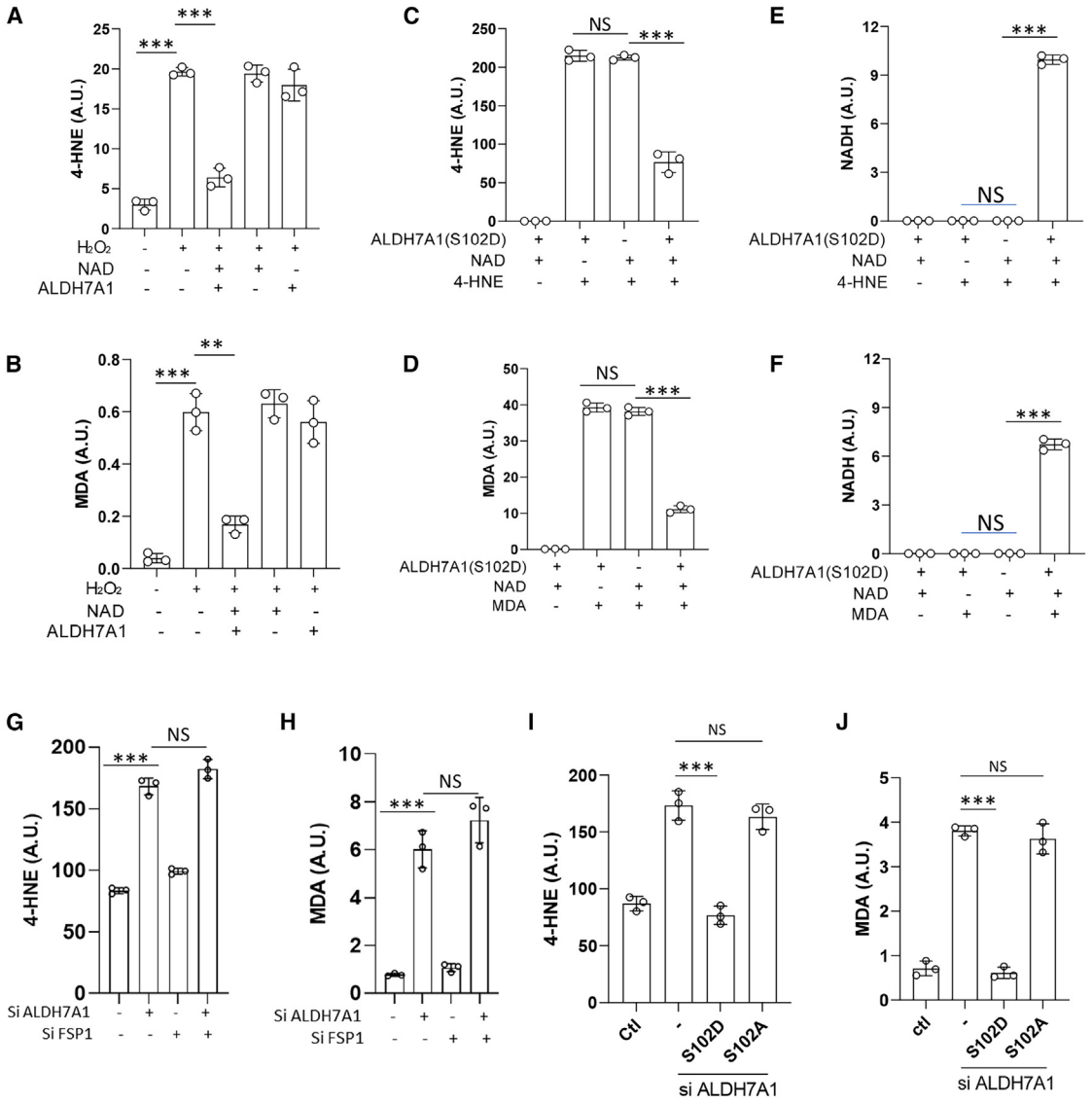

Figure 5. ALDH7A1 also protects against ferroptosis by consuming reactive aldehydes

(A–D) 4-HNE (A and C) or MDA (B and D) level was quantified upon the incubation of liposomes with different components as indicated, $n = 3$.
(E and F) NADH level was quantified upon the incubation of liposomes with different components as indicated, $n = 3$.
(G–J) 4-HNE (G and I) or MDA (H and J) level in MDA231 cells upon treatment as indicated, $n = 3$.
Quantitative data are shown as mean ± SD; $^{***}p < 0.0005$, $^{**}p < 0.005$, NS $p > 0.05$, Student's t test.

the lipid peroxidation, and the further addition of FSP1 decreased lipid peroxidation even more (Figure S4B). We also confirmed that the DTUN-induced lipid peroxidation provided substrates for ALDH7A1 activity, as simply adding ALDH7A1 in its membrane-bound form (S102D) along with NAD to the DTUN-exposed liposomes but without adding a substrate for ALDH7A1, resulted in NADH generation (Figure S4C). As control, incubation using liposomes not treated with DTUN did not generate NADH (Figure S4D). NADH also was not generated when NAD was not added (Figure S4E) or when the soluble form of ALDH7A1 (S102A) was used (Figure S4F). We also confirmed that DTUN-treated liposomes enabled FSP1 activity to be reconstituted, which required the wild-type FSP1 (Figure S4G) but not the catalytic-dead form (Figure S4H). Furthermore, the DTUN-treated liposomes generated the reactive aldehydes, 4-HNE (Figure S4I) and MDA (Figure S4J), whose levels were reduced upon the addition of ALDH7A1. Thus, the results from using DTUN to induce lipid peroxidation paralleled those using hydrogen peroxide as the inducer.

ALDH7A1 recruits FSP1 to membranes

We then uncovered a third way that ALDH7A1 protects against ferroptosis. The initial insight came from our attempt to reconstitute FSP1 activity. As a control, we incubated myristoylated

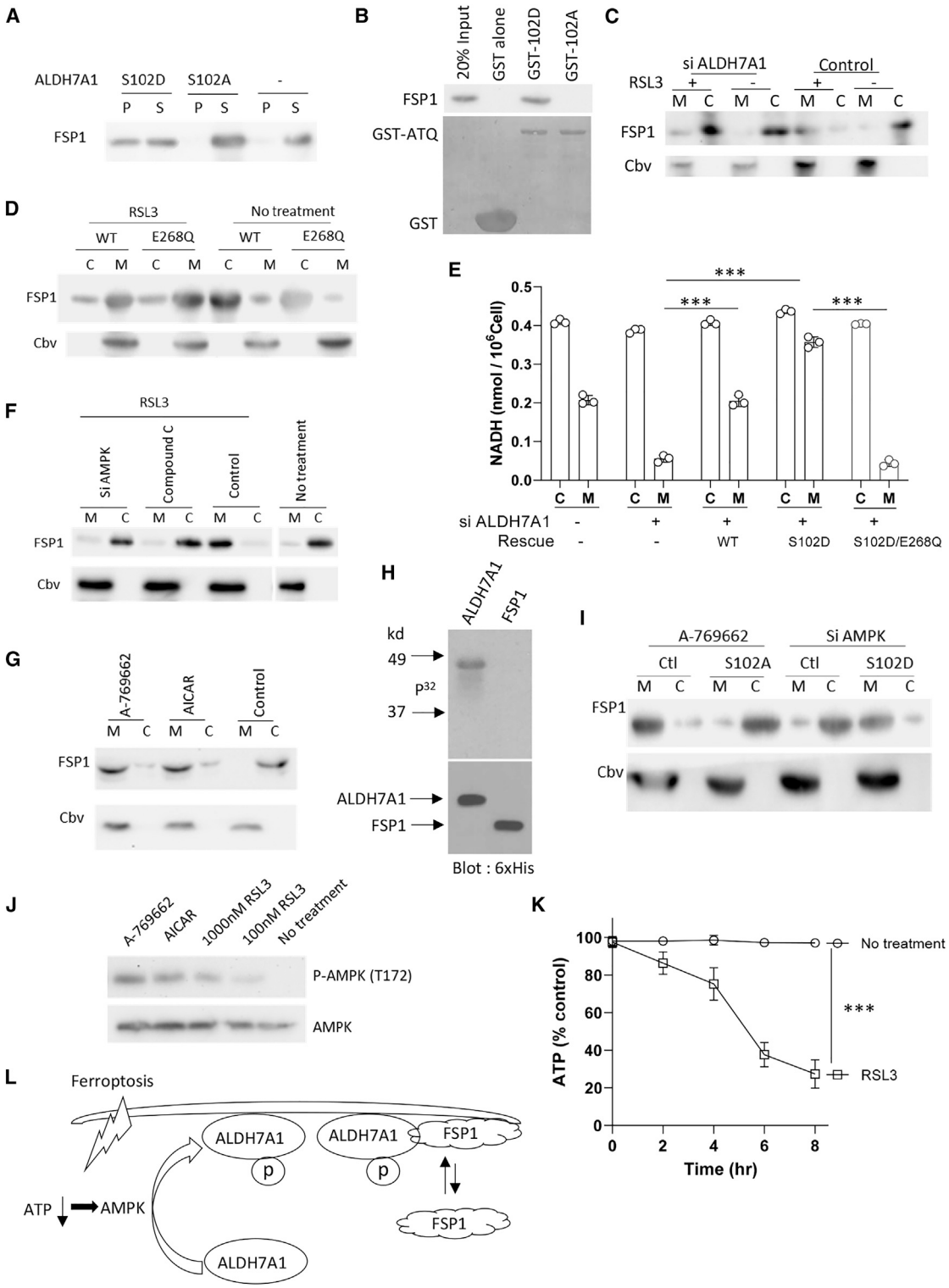

Figure 6. A signaling cascade regulates FSP1 recruitment to membrane

(A) FSP1 level on membrane (P) and in supernatant (S) upon the incubation of myristoylated FSP1 with liposomes and ALDH7A1 form as indicated, $n = 2$.

(B) Direct interaction between FSP1 and ALDH7A1 as glutathione S-transferase (GST) fusion proteins, as assessed by a pull-down experiment involving purified components, $n = 2$.

(C) FSP1 and Cbv levels on total membranes and in cytosol from MDA231 cells that were treated as indicated (RSL3, 100 nM), $n = 2$.

(legend continued on next page)

FSP1 alone with liposomes and discovered that it could not be recruited to these membranes (Figure 6A). Instead, the presence of ALDH7A1 was needed for FSP1 recruitment, which required the membrane-bound (S102D) but not the soluble (S102A) form of ALDH7A1 (Figure 6A). This finding also provided a way of assessing functionally the degree that our purified FSP1 was myristoylated. Whereas the wild type was completely recruited to liposomes, the mutant (G2A) remained completely soluble (Figure S5A), suggesting that the wild type form that we had generated was completely myristoylated. To further elucidate how ALDH7A1 recruits FSP1 to membrane, we found that the S102D form could interact directly with FSP1, while the S102A form could not (Figure 6B). Thus, besides its myristoylation, FSP1 must also interact with the membrane-bound (S102D) form of ALDH7A1 for stable recruitment to membranes.

We next confirmed that ALDH7A1 is also critical for the membrane localization of FSP1 in cells, as the replacement of endogenous ALDH7A1 with the S102D form promoted the membrane localization of FSP1, while the expression of the S102A form prevented this localization (Figure S5B). We also transfected FSP1 in cells for its overexpression and found that FSP1 recruitment was enhanced (Figure S5C), which suggested why previous studies that had transfected FSP1 seemingly detected FSP1 mostly on membranes by microscopy,[4,5] as this approach favors the detection of proteins on membranes over their cytosolic form.

We next found that increasing ferroptotic stress by RSL3 treatment induced the membrane recruitment of endogenous FSP1 in MDA231 cells, and notably this recruitment was prevented by siRNA against ALDH7A1 (Figure 6C). Similar findings were observed for multiple other cell types (Figures S5D–S5F). We also ruled out an alternate explanation that RSL3 treatment increased FSP1 expression (Figure S5G). Furthermore, siRNA against other ALDH members did not prevent the membrane recruitment of FSP1 induced by RSL3 treatment (Figure S5H), thus supporting the specificity by which ALDH7A1 recruits FSP1 to membranes.

The discovery that ALDH7A1 recruits FSP1 to membranes also suggested a way to determine whether FSP1 activity is the main consumer of membrane NADH in cells. We first confirmed that the membrane recruitment role of ALDH7A1 did not require its catalytic activity, as the expression of the catalytic-dead ALDH7A1 still supported the ability of RSL3 treatment to recruit FSP1 to membranes (Figure 6D). We then found that the expression of this mutant ALDH7A1 resulted in a markedly reduced level of membrane NADH (Figure 6E). Thus, by creating a condition in which FSP1 could be recruited to membranes, but ALDH7A1 could not generate membrane NADH, we have revealed that FSP1 activity is a dominant consumer of membrane NADH in cells.

A signaling mechanism regulating FSP1 activity

We next sought to elucidate how ferroptotic stress induces the membrane recruitment of FSP1 through ALDH7A1. Guided by our previous finding that the phosphorylation of the S102 residue in ALDH7A1 by AMP-activated protein kinase (AMPK) recruits ALDH7A1 to membrane,[13] we initially found that treating cells with an AMPK inhibitor, compound C, prevented RSL3 treatment from promoting the membrane recruitment of FSP1 (Figure 6F). Similar results were obtained when cells were treated with siRNA against AMPK (Figure 6F). Conversely, treatment with AMPK activators, either 5-aminoimidazole-4-carboxamide ribonucleotide (AICAR) or A-769662, resulted in FSP1 being recruited to membranes without the need for RSL3 treatment (Figure 6G).

We also performed an *in vitro* kinase assay to confirm that AMPK phosphorylates ALDH7A1 rather than FSP1 (Figure 6H). Moreover, to gather further support that ALDH7A1 mediates the ability of AMPK to regulate FSP1 recruitment, we found that AMPK activation could no longer induce FSP1 recruitment when the endogenous ALDH7A1 was replaced with the S102A form (Figure 6I). Conversely, when endogenous ALDH7A1 was replaced by the S102D form, siRNA against AMPK could no longer redistribute membrane FSP1 to the cytosol (Figure 6I).

To complement these biochemical findings, we next pursued morphologic analysis using confocal microscopy. We first confirmed the specificity of the antibodies used to detect endogenous FSP1, as immunostaining was abolished in FSP1 KO cells (Figure S6A). We then found that RSL3 treatment enhanced the colocalization of ALDH7A1 and FSP1 (Figure S6B). Furthermore, treatment with compound C or siRNA against AMPK prevented the ability of RSL3 treatment to promote this colocalization (Figure S6C), while treatment with AICAR or A-769662 bypassed the need for RSL3 treatment in enhancing the colocalization (Figure S6D).

To elucidate the membrane compartments that have recruited ALDH7A1 and FSP1, we next performed colocalization studies using organelle markers and detected both ALDH7A1 and FSP1 at similar levels on the plasma membrane (Figure S7A), endoplasmic reticulum (Figure S7B), the Golgi complex (Figure S7C), and lipid droplets (Figure S7D). Moreover, ferroptotic stress enhanced the recruitment of both proteins to these organelles, except for the ER (Figure S7B).

We then sought insight into how ferroptotic stress activates AMPK. A variety of energy stresses can activate AMPK, which can be detected by the phosphorylation of its T172 residue.[29]

(D) FSP1 and Cbv levels on total membranes and in cytosol from MDA231 cells that expressed different ALDH7A1 forms and treated as indicated (RSL3, 100 nM), $n = 2$.
(E) NADH level in total membranes and cytosol from MDA231 cells that express different forms of ALDH7A1 as indicated, $n = 3$.
(F and G) FSP1 and Cbv levels on total membranes and in cytosol from MDA231 cells that were treated as indicated (RSL3, 100 nM), $n = 2$.
(H) Assessing phosphorylation of ALDH7A1 and FSP1 by AMPK by an *in vitro* kinase assay, $n = 2$. Upper panel shows P^{32} incorporation.
(I) FSP1 and Cbv levels on total membranes and in cytosol from MDA231 cells that expressed different ALDH7A1 forms and treated as indicated, $n = 2$.
(J) AMPK phosphorylation in MDA231 cells that were treated as indicated, $n = 2$.
(K) Total ATP level in MDA231 cells that were treated as indicated (RSL3, 100 nM), $n = 3$.
(L) Summarizing how ferroptosis induction recruits ALDH7A1 and FSP1 to membranes.
Quantitative data are shown as mean ± SD; ***$p < 0.0005$, Student's t test.
See also Figures S5, S6, and S7.

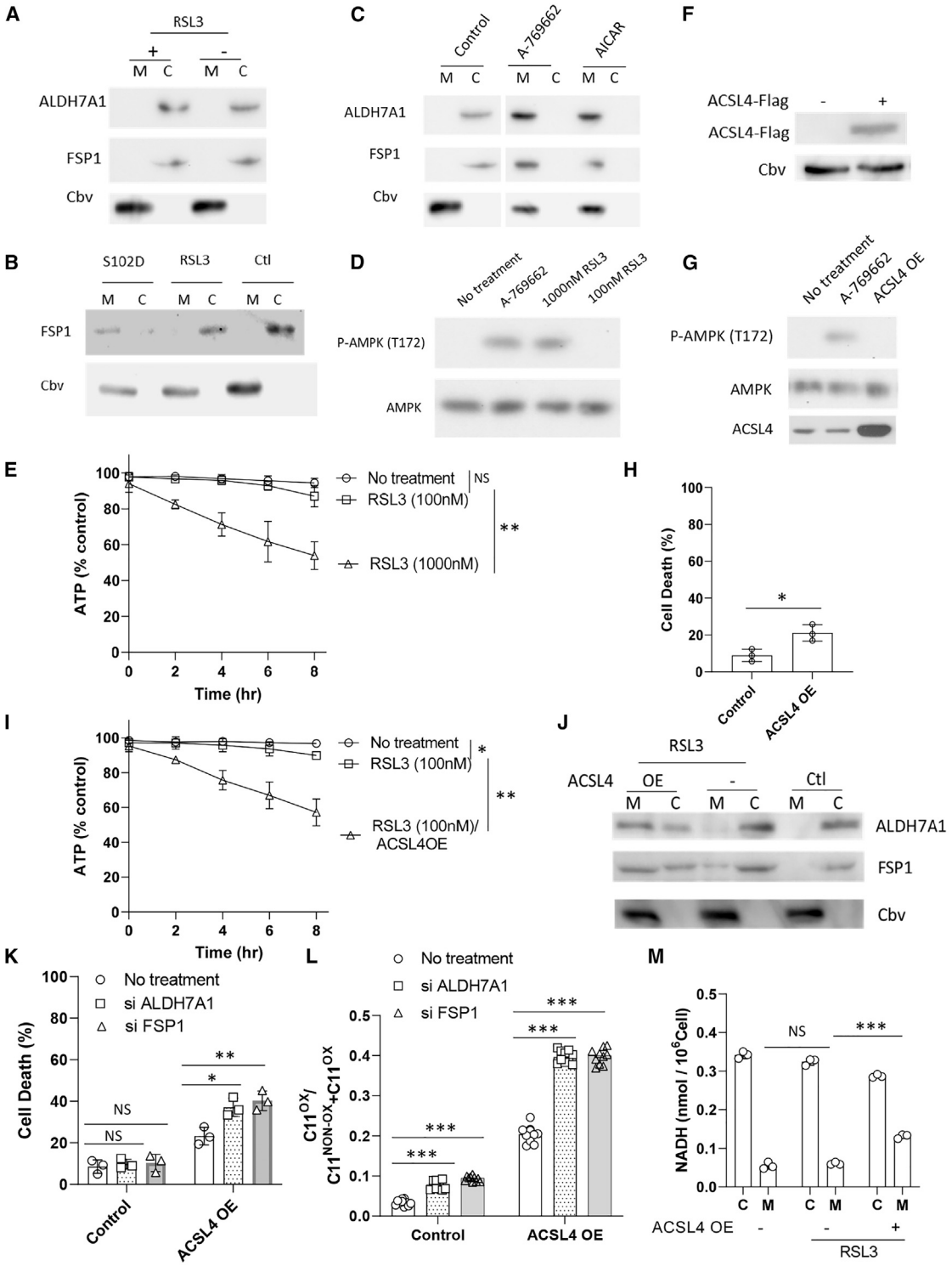

Figure 7. Higher ferroptotic stress is needed to activate the signaling cascade in H460 cells

(A) ALDH7A1, FSP1, and Cbv levels on total membranes and in cytosol from H460 cells that were treated as indicated (RSL3, 100 nM), $n = 2$.

(B) FSP1 and Cbv levels on total membranes and in cytosol from H460 cells that expressed ALDH7A1 form and treated (RSL3, 100 nM) as indicated, $n = 2$.

(C) ALDH7A1, FSP1, and Cbv levels on total membranes and in cytosol from H460 cells that were treated as indicated, $n = 2$.

(D) AMPK phosphorylation in H460 cells that were treated as indicated, $n = 2$.

(E) Total ATP level in H460 cells that were treated as indicated, $n = 3$.

(legend continued on next page)

We found that RSL3 treatment enhanced AMPK phosphorylation at this residue (Figure 6J). Furthermore, RSL3 treatment decreased the cellular ATP level (Figure 6K). Thus, the findings altogether revealed a signaling cascade that regulates the membrane recruitment of FSP1 by ALDH7A1. Upon the induction of ferroptotic stress, the cellular ATP level becomes decreased, which activates AMPK to phosphorylate ALDH7A1 that then results in ALDH7A1 being localized to membranes for the stable recruitment of FSP1 (summarized in Figure 6L). A key implication of this mechanism is that, rather than operating constitutively, FSP1 activity is regulated, being activated acutely by ferroptotic stress through signaling.

Susceptibility to ferroptosis regulates the activation of the signaling mechanism

We next noted that a previous survey of cell types had found that the expression level of FSP1 largely correlates with the degree that cells are dependent on FSP1 for protection against ferroptosis.[4] However, some cells, such as H460, only showed FSP1 dependency when high level of ferroptotic stress was induced.[4] Thus, we wondered whether the signaling mechanism that we have elucidated may shed insight into an explanation.

We initially found that ferroptotic stress induced by the usual dose of RSL3 treatment (100 nM) could not promote the membrane recruitment of either ALDH7A1 or FSP1 in H460 cells (Figure 7A), consistent with a defect in the signaling cascade. To pinpoint the defect, we next replaced the endogenous ALDH7A1 with the S102D form and found that FSP1 could be recruited to membranes without the need for RSL3 treatment (Figure 7B), suggesting that the ability of ALDH7A1 to recruit FSP1 was intact in these cells. We next activated AMPK pharmacologically and found that FSP1 could be recruited to membrane without RSL3 treatment (Figure 7C). Thus, this part of the signaling cascade was also intact. We then found that the usual dose of RSL3 treatment (100 nM) could not activate AMPK, but rather, high-dose RSL3 treatment (1 μM) was needed, as reflected by AMPK phosphorylation at its T172 residue (Figure 7D). This higher dose of RSL3 treatment was also needed to reduce the cellular ATP level (Figure 7E). Thus, the collective results revealed that ferroptotic stress has impaired ability to reduce the cellular ATP level in H460 cells.

To further characterize this defect, we were led by our survey above of cell types that had revealed H460 and MCF7 cells to have similarly low susceptibility to ferroptotic stress and low membrane NADH level. As such, we explored whether, like the case of MCF7 cells, overexpressing ACSL4 in H460 cells would also increase their susceptibility to ferroptotic stress. We initially confirmed that ACSL4 overexpression (Figure 7F), by itself, did not activate the signaling cascade, as assessed by AMPK activation (Figure 7G). Rather, ACSL4 overexpression resulted in H460 cells becoming more susceptible to ferroptotic stress, as reflected by enhanced cell death when treated with the standard dose (100 nM) of RSL3 (Figure 7H). This treatment also decreased the cellular ATP level (Figure 7I) and induced FSP1 recruitment to membranes (Figure 7J).

We next found that this conversion of H460 cells resulted in them being more dependent on ALDH7A1 and FSP1 for protection against ferroptosis, as assessed by cell death (Figure 7K) and lipid peroxidation (Figure 7L). Moreover, this increased dependency was associated with higher level of membrane NADH (Figure 7M). Thus, the results altogether suggested a nuanced explanation for how H460 cells are dependent on FSP1 for protection against ferroptotic stress. Because they normally express relatively low level of ACSL4, they are relatively resistant to ferroptotic stress. However, when faced with high level of ferroptotic stress, their dependence on FSP1 for protection becomes apparent.

DISCUSSION

We have advanced a fundamental understanding of NADH. Whereas its currently known roles involve the soluble form, we find that NADH exists at significant levels on cellular membranes. Further characterizing this previously unappreciated pool, we find that membrane NADH is maintained by binding to both proteins and lipids on membranes. The latter is surprising, as NADH has not been expected to bind directly to lipids. We then find that membrane NADH level is controlled by ALDH7A1 activity. We also find that membrane NADH behaves as a distinct pool from soluble NADH and elucidate a mechanism to explain how these two pools are compartmentalized.

Having defined these key properties of membrane NADH, we then identified its function, finding that membrane NADH generated by ALDH7A1 supports FSP1 activity. This conclusion is supported initially by cell-based studies and then more definitively through reconstitution studies that use purified components. In this regard, although a recent study has suggested that ALDH1A3 supports FSP1 activity by generating NADH,[30] only cell-based studies were done, and thus indirect effects cannot be ruled out. The reconstitution approach has also enabled us to elucidate a second way that ALDH7A1 protects against ferroptosis. Upon reconstituting lipid peroxidation, we find that simply reconstituting ALDH7A1 activity affords partial protection against lipid peroxidation. Characterizing this FSP1-independent mechanism, we find that ALDH7A1 activity consumes reactive aldehydes on membranes. Thus, whereas the

(F) Confirming the expression of transfected ACSL4 in H460 cells, $n = 2$.
(G) AMPK phosphorylation in H460 cells that were treated or transfected as indicated, $n = 2$.
(H) Cell death was quantified for H460 cells that were transfected as indicated and treated with RSL3 (100 nM), $n = 3$.
(I) Total ATP level in H460 cells that were treated as indicated, $n = 3$.
(J) ALDH7A1, FSP1, and Cbv levels on total membranes and cytosol from H460 cells that were transfected and treated as indicated (RSL3, 100 nM), $n = 2$.
(K) Cell death was quantified for H460 cells that were treated as indicated, $n = 3$.
(L) Lipid peroxidation was quantified for H460 cells that were treated as indicated, $n = 2$. A representative experiment is shown.
(M) NADH level in total membranes and cytosol from H460 cells that were treated as indicated (RSL3, 100 nM), $n = 3$.
Quantitative data are shown as mean ± SD; $^{***}p < 0.0005$, $^{**}p < 0.005$, $^{*}p < 0.05$, NS $p > 0.05$, Student's t test.

only well-established physiologic substrate of ALDH7A1 is an intermediate in lysine metabolism,[12] our finding that ALDH7A1 activity can be reconstituted simply by inducing lipid peroxidation implicates many more physiologic substrates of ALDH7A1 activity than currently appreciated.

We have discovered yet a third way that ALDH7A1 protects against ferroptosis, which involves regulating FSP1 recruitment to membrane. This finding has led us to reveal a signaling mechanism that regulates FSP1 activity, which introduces a new paradigm in the understanding of how FSP1 acts. Rather than operating constitutively, FSP1 activity is regulated, being activated by ferroptotic stress.

We have also shed insight into why cells exhibit varying levels of membrane NADH and dependency on FSP1 for protection against ferroptosis. When cells are less susceptible to ferroptosis, such as having low ACSL4 level, membrane NADH level is relatively low because cells are less dependent on FSP1 for protection. In contrast, when cells are more susceptible to ferroptosis, as seen with higher ACSL4 expression levels, membrane NADH levels become higher because FSP1 activity takes on greater importance. A general implication of these findings is that cells cannot be viewed simply as being either FSP1-dependent or FSP1-independent, but rather, acting along a continuum, having the capacity to recruit the FSP1 mechanism when ferroptotic stress becomes overwhelming. As such, we have advanced a fundamental understanding of not only how NADH acts but also how the cell protects against ferroptosis.

Limitations of the study

We have examined a variety of cell lines to suggest that our findings are generalizable. However, a more extensive survey of cell types will be needed for definitive confirmation. Further studies will also be needed to provide a better understanding of other key findings. We have found that NAD, like NADH, also exists at significant levels on membrane with ALDH7A1 activity likely converting membrane NAD to membrane NADH. Thus, how membrane NAD is generated will need to be defined. We have also found that ferroptotic stress enhances the recruitment of both ALDH7A1 and FSP1 to multiple intracellular compartments. An exception is their ER distribution, and thus future studies will be needed to explain this anomaly. We have further discovered that the myristoylation of FSP1 is not sufficient for its membrane recruitment. Rather, FSP1 must also interact with the phosphorylated form of ALDH7A1. A mechanistic implication of this finding is that the dephosphorylation of ALDH7A1 would release FSP1 from membrane, and thus future studies will also be needed to identify the phosphatase that is predicted to trigger this release.

RESOURCE AVAILABILITY

Lead contact

Further information and requests for resources and reagents should be directed to and will be fulfilled by the lead contact, Victor Hsu (vhsu@bwh.harvard.edu).

Materials availability

All unique/stable reagents generated in this study are available from the lead contact upon reasonable request.

Data and code availability

Microscopy data will be shared by the lead contact upon request. Software and algorithms used in this study are listed in key resources table. Any additional information required to reanalyze the data reported in this paper is available from the lead contact upon request.

ACKNOWLEDGMENTS

We thank Jian Li for advice and discussions. This work was supported by funding to V.W.H. (NIH grant R37GM058615), A.J.M. (VA grants IK6 BX006469 and I01 BX005637), M.C. (the Deutsche Forschungsgemeinschaft/DFG [CO 291/7-1, the Priority Program SPP 2306; CO 291/9-1, #461385412; CO 291/10-1, #461507177], the CRC TRR 353 [CO 291/11-1/#471011418], the German Federal Ministry of Education and Research [BMBF] FERROPATH [01EJ2205B], and the European Research Council [ERC] under the European Union's Horizon 2020 research and innovation programme [grant agreement no. GA 884754]), Y.M. (JST Moonshot R&D: JPMJMS2022), K.K. (JSPS KAKENHI: 24K18515), J.L. (NIH grants U01HG007691, R01HL155107, R01HL155096, and R01HL166137; AHA grants 957729 and 24MERIT1185447; and EU grant HorizonHealth2021 101057619), and W.M.O. (NIH grants R01HL167718 and K08HL128802).

AUTHOR CONTRIBUTIONS

J.-S.Y. performed most cell-based studies and all reconstitution studies. V.W.H. conceived and supervised the project. W.S.H., K.K., J.S., and Y.M. performed animal studies. J.C. and A.J.M. performed ubiquinone/ubiquinol analyses. W.M.O. and J.L. performed cell-based flux studies. T.N., E.M., and M.C. provided HT1080 and H460 cell variants and helpful discussions. All authors contributed to data interpretation and provided feedback on the manuscript.

DECLARATION OF INTERESTS

M.C. is a co-founder and shareholder of ROSCUE Therapeutics GmbH.

STAR★METHODS

Detailed methods are provided in the online version of this paper and include the following:

- KEY RESOURCES TABLE
- EXPERIMENTAL MODEL AND STUDY PARTICIPANT DETAILS
  - Cells
  - Animals
- METHOD DETAILS
  - Chemicals
  - Antibodies
  - Plasmids
  - Purification of recombinant proteins
  - Transfection and siRNA
  - Subcellular fractionation
  - Membrane treatments
  - Frex biosensor measurement
  - Extracellular flux measurement
  - Lipid peroxidation measurement
  - Ubiquinone/ubiquinol measurement
  - Protein interaction assays
  - In vitro kinase assay
  - Colocalization studies
  - Reconstitution of ALDH7A1 and FSP1 activities
  - Reconstitution of lipid peroxidation
  - Other assays
- QUANTIFICATION AND STATISTICAL ANALYSIS

Received: July 3, 2024
Revised: December 19, 2024
Accepted: March 10, 2025
Published: April 14, 2025

REFERENCES

1. Stockwell, B.R., Friedmann Angeli, J.P., Bayir, H., Bush, A.I., Conrad, M., Dixon, S.J., Fulda, S., Gascón, S., Hatzios, S.K., Kagan, V.E., et al. (2017). Ferroptosis: A Regulated Cell Death Nexus Linking Metabolism, Redox Biology, and Disease. Cell *171*, 273–285. https://doi.org/10.1016/j.cell.2017.09.021.
2. Yang, W.S., SriRamaratnam, R., Welsch, M.E., Shimada, K., Skouta, R., Viswanathan, V.S., Cheah, J.H., Clemons, P.A., Shamji, A.F., Clish, C.B., et al. (2014). Regulation of ferroptotic cancer cell death by GPX4. Cell *156*, 317–331. https://doi.org/10.1016/j.cell.2013.12.010.
3. Seiler, A., Schneider, M., Förster, H., Roth, S., Wirth, E.K., Culmsee, C., Plesnila, N., Kremmer, E., Rådmark, O., Wurst, W., et al. (2008). Glutathione peroxidase 4 senses and translates oxidative stress into 12/15-lipoxygenase dependent- and AIF-mediated cell death. Cell Metab. *8*, 237–248. https://doi.org/10.1016/j.cmet.2008.07.005.
4. Doll, S., Freitas, F.P., Shah, R., Aldrovandi, M., da Silva, M.C., Ingold, I., Goya Grocin, A., Xavier da Silva, T.N., Panzilius, E., Scheel, C.H., et al. (2019). FSP1 is a glutathione-independent ferroptosis suppressor. Nature *575*, 693–698. https://doi.org/10.1038/s41586-019-1707-0.
5. Bersuker, K., Hendricks, J.M., Li, Z., Magtanong, L., Ford, B., Tang, P.H., Roberts, M.A., Tong, B., Maimone, T.J., Zoncu, R., et al. (2019). The CoQ oxidoreductase FSP1 acts parallel to GPX4 to inhibit ferroptosis. Nature *575*, 688–692. https://doi.org/10.1038/s41586-019-1705-2.
6. Stryer, L. (1995). Part III. Metabolic energy: generation and storage. In Biochemistry (W.H. Freeman), pp. 441–682.
7. Marchitti, S.A., Brocker, C., Stagos, D., and Vasiliou, V. (2008). Non-P450 aldehyde oxidizing enzymes: the aldehyde dehydrogenase superfamily. Expert Opin. Drug Metab. Toxicol. *4*, 697–720. https://doi.org/10.1517/17425255.4.6.697.
8. Rodríguez-Zavala, J.S., Calleja, L.F., Moreno-Sánchez, R., and Yoval-Sánchez, B. (2019). Role of Aldehyde Dehydrogenases in Physiopathological Processes. Chem. Res. Toxicol. *32*, 405–420. https://doi.org/10.1021/acs.chemrestox.8b00256.
9. Shortall, K., Djeghader, A., Magner, E., and Soulimane, T. (2021). Insights into Aldehyde Dehydrogenase Enzymes: A Structural Perspective. Front. Mol. Biosci. *8*, 659550. https://doi.org/10.3389/fmolb.2021.659550.
10. Lee, P., Kuhl, W., Gelbart, T., Kamimura, T., West, C., and Beutler, E. (1994). Homology between a human protein and a protein of the green garden pea. Genomics *21*, 371–378. https://doi.org/10.1006/geno.1994.1279.
11. Guerrero, F.D., Jones, J.T., and Mullet, J.E. (1990). Turgor-responsive gene transcription and RNA levels increase rapidly when pea shoots are wilted. Sequence and expression of three inducible genes. Plant Mol. Biol. *15*, 11–26. https://doi.org/10.1007/BF00017720.
12. Mills, P.B., Struys, E., Jakobs, C., Plecko, B., Baxter, P., Baumgartner, M., Willemsen, M.A.A.P., Omran, H., Tacke, U., Uhlenberg, B., et al. (2006). Mutations in antiquitin in individuals with pyridoxine-dependent seizures. Nat. Med. *12*, 307–309. https://doi.org/10.1038/nm1366.
13. Yang, J.S., Hsu, J.W., Park, S.Y., Lee, S.Y., Li, J., Bai, M., Alves, C., Tseng, W., Michelet, X., Ho, I.C., et al. (2019). ALDH7A1 inhibits the intracellular transport pathways during hypoxia and starvation to promote cellular energy homeostasis. Nat. Commun. *10*, 4068. https://doi.org/10.1038/s41467-019-11932-0.
14. Yang, J.S., Lee, S.Y., Spanò, S., Gad, H., Zhang, L., Nie, Z., Bonazzi, M., Corda, D., Luini, A., and Hsu, V.W. (2005). A role for BARS at the fission step of COPI vesicle formation from Golgi membrane. EMBO J. *24*, 4133–4143. https://doi.org/10.1038/sj.emboj.7600873.
15. Yang, J.S., Zhang, L., Lee, S.Y., Gad, H., Luini, A., and Hsu, V.W. (2006). Key components of the fission machinery are interchangeable. Nat. Cell Biol. *8*, 1376–1382. https://doi.org/10.1038/ncb1503.
16. Zhao, Y., Jin, J., Hu, Q., Zhou, H.M., Yi, J., Yu, Z., Xu, L., Wang, X., Yang, Y., and Loscalzo, J. (2011). Genetically encoded fluorescent sensors for intracellular NADH detection. Cell Metab. *14*, 555–566. https://doi.org/10.1016/j.cmet.2011.09.004.
17. Titov, D.V., Cracan, V., Goodman, R.P., Peng, J., Grabarek, Z., and Mootha, V.K. (2016). Complementation of mitochondrial electron transport chain by manipulation of the NAD^+/NADH ratio. Science *352*, 231–235. https://doi.org/10.1126/science.aad4017.
18. Slee, E.A., Zhu, H., Chow, S.C., MacFarlane, M., Nicholson, D.W., and Cohen, G.M. (1996). Benzyloxycarbonyl-Val-Ala-Asp (OMe) fluoromethylketone (Z-VAD.FMK) inhibits apoptosis by blocking the processing of CPP32. Biochem. J. *315*, 21–24. https://doi.org/10.1042/bj3150021.
19. Degterev, A., Huang, Z., Boyce, M., Li, Y., Jagtap, P., Mizushima, N., Cuny, G.D., Mitchison, T.J., Moskowitz, M.A., and Yuan, J. (2005). Chemical inhibitor of nonapoptotic cell death with therapeutic potential for ischemic brain injury. Nat. Chem. Biol. *1*, 112–119. https://doi.org/10.1038/nchembio711.
20. Dixon, S.J., Lemberg, K.M., Lamprecht, M.R., Skouta, R., Zaitsev, E.M., Gleason, C.E., Patel, D.N., Bauer, A.J., Cantley, A.M., Yang, W.S., et al. (2012). Ferroptosis: an iron-dependent form of nonapoptotic cell death. Cell *149*, 1060–1072. https://doi.org/10.1016/j.cell.2012.03.042.
21. Doll, S., Proneth, B., Tyurina, Y.Y., Panzilius, E., Kobayashi, S., Ingold, I., Irmler, M., Beckers, J., Aichler, M., Walch, A., et al. (2017). ACSL4 dictates ferroptosis sensitivity by shaping cellular lipid composition. Nat. Chem. Biol. *13*, 91–98. https://doi.org/10.1038/nchembio.2239.
22. Kagan, V.E., Mao, G., Qu, F., Angeli, J.P.F., Doll, S., Croix, C.S., Dar, H.H., Liu, B., Tyurin, V.A., Ritov, V.B., et al. (2017). Oxidized arachidonic and adrenic PEs navigate cells to ferroptosis. Nat. Chem. Biol. *13*, 81–90. https://doi.org/10.1038/nchembio.2238.
23. Mishima, E., Ito, J., Wu, Z., Nakamura, T., Wahida, A., Doll, S., Tonnus, W., Nepachalovich, P., Eggenhofer, E., Aldrovandi, M., et al. (2022). A non-canonical vitamin K cycle is a potent ferroptosis suppressor. Nature *608*, 778–783. https://doi.org/10.1038/s41586-022-05022-3.
24. Nakamura, T., Hipp, C., Santos Dias Mourão, A., Borggräfe, J., Aldrovandi, M., Henkelmann, B., Wanninger, J., Mishima, E., Lytton, E., Emler, D., et al. (2023). Phase separation of FSP1 promotes ferroptosis. Nature *619*, 371–377. https://doi.org/10.1038/s41586-023-06255-6.
25. Gaschler, M.M., Andia, A.A., Liu, H., Csuka, J.M., Hurlocker, B., Vaiana, C.A., Heindel, D.W., Zuckerman, D.S., Bos, P.H., Reznik, E., et al. (2018). $FINO_2$ initiates ferroptosis through GPX4 inactivation and iron oxidation. Nat. Chem. Biol. *14*, 507–515. https://doi.org/10.1038/s41589-018-0031-6.
26. Nakamura, T., Mishima, E., Yamada, N., Mourão, A.S.D., Trümbach, D., Doll, S., Wanninger, J., Lytton, E., Sennhenn, P., Nishida Xavier da Silva, T., et al. (2023). Integrated chemical and genetic screens unveil FSP1 mechanisms of ferroptosis regulation. Nat. Struct. Mol. Biol. *30*, 1806–1815. https://doi.org/10.1038/s41594-023-01136-y.
27. Ayala, A., Muñoz, M.F., and Argüelles, S. (2014). Lipid peroxidation: production, metabolism, and signaling mechanisms of malondialdehyde and 4-hydroxy-2-nonenal. Oxid. Med. Cell. Longev. *2014*, 360438. https://doi.org/10.1155/2014/360438.
28. Shah, R., Farmer, L.A., Zilka, O., Van Kessel, A.T.M., and Pratt, D.A. (2019). Beyond DPPH: Use of Fluorescence-Enabled Inhibited Autoxidation to Predict Oxidative Cell Death Rescue. Cell Chem. Biol. *26*, 1594–1607.e7. https://doi.org/10.1016/j.chembiol.2019.09.007.
29. Hardie, D.G., Ross, F.A., and Hawley, S.A. (2012). AMPK: a nutrient and energy sensor that maintains energy homeostasis. Nat. Rev. Mol. Cell Biol. *13*, 251–262. https://doi.org/10.1038/nrm3311.
30. Cui, W., Guo, M., Liu, D., Xiao, P., Yang, C., Huang, H., Liang, C., Yang, Y., Fu, X., Zhang, Y., et al. (2024). Gut microbial metabolite facilitates colorectal cancer development via ferroptosis inhibition. Nat. Cell Biol. *26*, 124–137. https://doi.org/10.1038/s41556-023-01314-6.

31. Moreb, J.S., Baker, H.V., Chang, L.J., Amaya, M., Lopez, M.C., Ostmark, B., and Chou, W. (2008). ALDH isozymes downregulation affects cell growth, cell motility and gene expression in lung cancer cells. Mol. Cancer *7*, 87. https://doi.org/10.1186/1476-4598-7-87.

32. Tiedemann, R.E., Zhu, Y.X., Schmidt, J., Shi, C.X., Sereduk, C., Yin, H., Mousses, S., and Stewart, A.K. (2012). Identification of molecular vulnerabilities in human multiple myeloma cells by RNA interference lethality screening of the druggable genome. Cancer Res. *72*, 757–768. https://doi.org/10.1158/0008-5472.CAN-11-2781.

33. Yang, J.S., Hsu, J.W., Park, S.Y., Li, J., Oldham, W.M., Beznoussenko, G.V., Mironov, A.A., Loscalzo, J., and Hsu, V.W. (2018). GAPDH inhibits intracellular pathways during starvation for cellular energy homeostasis. Nature *561*, 263–267. https://doi.org/10.1038/s41586-018-0475-6.

34. Lu, J., Chen, J., Xu, N., Wu, J., Kang, Y., Shen, T., Kong, H., Ma, C., Cheng, M., Shao, Z., et al. (2016). Activation of AIFM2 enhances apoptosis of human lung cancer cells undergoing toxicological stress. Toxicol. Lett. *258*, 227–236. https://doi.org/10.1016/j.toxlet.2016.07.002.

35. Li, Y., Feng, D., Wang, Z., Zhao, Y., Sun, R., Tian, D., Liu, D., Zhang, F., Ning, S., Yao, J., et al. (2019). Ischemia-induced ACSL4 activation contributes to ferroptosis-mediated tissue injury in intestinal ischemia/reperfusion. Cell Death Differ. *26*, 2284–2299. https://doi.org/10.1038/s41418-019-0299-4.

STAR★METHODS

KEY RESOURCES TABLE

REAGENT or RESOURCE	SOURCE	IDENTIFIER
Antibodies		
Rabbit anti-ALDH7A1 (WB 1:1000, IF 1:500)	This lab	N/A
Rabbit anti-FSP1 (WB 1:5000, IF 1:200)	Proteintech	20886-1-AP; RRID:AB_2878756
Rabbit anti-β-actin (WB 1:1000)	Cell signaling	8456: RRID:AB_10998774
Rabbit anti-cellubrevin (Cbv, WB 1:1000)	This lab	N/A
Mouse anti-GAPDH (WB 1:1000)	Invitrogen	AM4300: RRID:AB_2536381
Flag epitope (WB 1:1000)	Invitrogen	MA1-91878; RRID:AB_1957945
HA epitope (WB 1:200)	Santa Cruz	sc-7392; RRID:AB_627809
Myc epitope (WB 1:200)	This lab	N/A
Mouse monoclonal anti-GFP (WB 1:1000)	Thermo Scientific	MA5-15256; RRID:AB_10979281
Mouse monoclonal anti-FSP1 (AMID,WB 1:500)	Santa Cruz	sc-377120; RRID:AB_2893240
Mouse monoclonal anti-ACSL4 (WB 1:100)	Santa Cruz	sc-271800; RRID:AB_10715092
Mouse monoclonal anti-COX4 (WB 1:100)	Santa Cruz	sc-376731; RRID:AB_2904544
Mouse monoclonal anti-Coatomer (IF 1:10)	James Rothman (Yale)	CM1A10
Rabbit anti-AMPKα1 (WB 1:500)	Cell signaling	2603S; RRID:AB_490795
Rabbit anti-phospho-substrates of AMPK (WB 1:500)	Cell signaling	5759S; RRID:AB_10949320
Rabbit anti-6xHis epitope (WB 1:1000)	Santa Cruz	sc-8036; RRID:AB_627727
Rabbit anti-GFP (WB 1:1000)	Thermo Scientific	MA5-15256; RRID:AB_10979281
Rabbit anti-GST (WB 1:1000)	Santa Cruz	sc-138; RRID:AB_627677
Rabbit anti-GM130 (WB 1:1000)	Sigma-Aldrich	G7295; RRID:AB_532244
Rabbit anti-Sec61 (WB 1:1000)	Abcam	ab15576; RRID:AB_301985
Mouse anti-Na-K ATPase (WB: 1:50)	Abcam	N/A
Mouse monoclonal anti-Calnexin (AF8) (WB: 1:100)	Michael Brenner (Harvard)	N/A
Rabbit anti-Lamp1 (WB: 1:100)	Abcam	ab24170; RRID:AB_775978
HRP donkey anti-mouse IgG (WB 1:10,000)	Jackson ImmunoResearch	715-035150; RRID: AB_2340770
HRP donkey anti-rabbit IgG (WB 1:10,000)	Jackson ImmunoResearch	711-035-152; RRID: AB_10015282
Cy2 donkey anti-mouse IgG (IF 1:200)	Jackson ImmunoResearch	715-545-150; AB_2340846
Cy2 donkey anti-rabbit IgG (IF 1:200)	Jackson ImmunoResearch	711- 545-152: AB_2340846
Cy3 goat anti-mouse IgG (IF 1:200)	Jackson ImmunoResearch	115-165-062; RRID: AB_2338685
Cy3 donkey anti-rabbit IgG (IF 1:200)	Jackson ImmunoResearch	711-165-152; RRID: AB_2307443
Cy3 donkey anti-sheep IgG (IF 1:200)	Jackson ImmunoResearch	713-165-147; RRID: AB_2315778
Bacterial and virus strains		
BL21	Thermo Scientific	EC0114
DH5α	Thermo Scientific	18265017
Chemicals, peptides, and recombinant proteins		
NAD	Sigma-Aldrich	N0632
NADH	Sigma-Aldrich	N8129
Hydrogen peroxide	Sigma-Aldrich	H1009
Octanal	Sigma-Aldrich	O5608
Rotenone	Sigma-Aldrich	557368
Ubiquinone	Sigma-Aldrich	C9538
Antimycin A	Sigma-Aldrich	A8674
A-769662	Cayman Chemicals	11900

(*Continued on next page*)

Continued

REAGENT or RESOURCE	SOURCE	IDENTIFIER
AICAR	Cell signaling	9944
RSL3	Cayman Chemicals	19288
Erastin	Cayman Chemicals	17754
Liproxstatin-1	Sigma-Aldrich	950455-15-9
Ferrostatin-1	Cayman Chemicals	17729
DFO	Cayman Chemicals	14595
FINO2	Cayman Chemicals	25096
Z-VAD-FMK	Cayman Chemicals	14467
Necrostatin-1	Cayman Chemicals	11658
4-HNE	Sigma-Aldrich	393204
MDA	Sigma-Aldrich	SMB00976
DTUN	Cayman Chemicals	32742
Cholesterol	Avanti Polar Lipids	700100
Sphingomyelin	Avanti Polar Lipids	860061
Dioleoyl-phosphatidylcholine (DOPC)	Avanti Polar Lipids	850375
Dioleoyl-phosphatidylethanolamine (DOPE)	Avanti Polar Lipids	850725
Dioleoyl-phosphatidylserine (DOPS)	Avanti Polar Lipids	840035
Dioleoyl-phosphatidylinositol (DOPI)	Avanti Polar Lipids	850149
Phosphatidic acid (PA)	Avanti Polar Lipids	840875
1-stearoyl-2-arachidonoyl-sn-glycero-3-phosphoethanolamine (PUFA-PE)	Avanti Polar Lipids	850804
C11 BODIPY 581/591	Invitrogen	D-3861
FM4-64FX	Invitrogen	F34653
LipidSpot 488 Lipid Droplet stain	Biotium	70065
Recombinant ALDH7A1	Yang et al.[13]	N/A
Recombinant myristoylated FSP1	This paper	N/A
Critical commercial assays		
NAD/NADH Measurement Kit	Sigma-Aldrich	MAK037
NADP/NADPH Measurement Kit	Sigma-Aldrich	MAK479
MDA Measurement Kit	Sigma-Aldrich	MAK058
4-HNE Measurement Kit	Abcam	ab238538
Mitochondria / Cytosol Fractionation Kit	Sigma-Aldrich	MIT1000
Site-directed mutagenesis kit Quickchange II	Agilent	200521
Phusion High-Fidelity PCR Master Mix with HF Buffer	Biolabs	M0531S
PrestoBlue Cell Viability Reagent	Invitrogen	A13261
Experimental models: Cell lines		
HeLa	ATCC	N/A
HEK 293	ATCC	N/A
MEF	ATCC	N/A
MDA-MB-231	Joan Brugge (Harvard)	N/A
MDA-MB-436	Joan Brugge (Harvard)	N/A
MDA-MB-453	Joan Brugge (Harvard)	N/A
MCF7	Joan Brugge (Harvard)	N/A
H460	Joan Brugge (Harvard)	N/A
A549	Joan Brugge (Harvard)	N/A
Primary synoviocytes	Michael Brenner (Harvard)	N/A
NIH-3T3	Michael Brenner (Harvard)	N/A
HT1080	Doll et al.[4,21]	N/A

(*Continued on next page*)

Continued

REAGENT or RESOURCE	SOURCE	IDENTIFIER
HT1080/GPX4 KO	Doll et al.[4,21]	N/A
HT1080/GPX4 KO/FSP1 OE	Doll et al.[4,21]	N/A
HT1080/ GPX4 KO/ FSP1 OE/ ALDH7A1 KO	This paper	N/A
H460 KO	Nakamura et al.[24]	N/A
Experimental models: Organisms/strains		
NSG mice	Jackson Laboratory	N/A
Oligonucleotides		
ALDH7A1 (E268Q) primer forward: 5′-gggagaagtctgttgcaacttggaggaaacaatgcc-3′	This paper	N/A
ALDH7A1 (E268Q) primer reverse: 5′-ggcattgtttcctccaagttgcaacagacttctccc-3	This paper	N/A
ALDH7A1 (S102A) primer forward: 5′-aagatccaagtactaggagccttggtgtctttggagatgggg-3′	This paper	N/A
ALDH7A1 (S102A) primer reverse: 5′-ccccatctccaaagacaccaaggctcctagtacttggatctt-3′	This paper	N/A
ALDH7A1 (S102D) primer forward: 5′-aagatccaagtactaggagacttggtgtctttggagatgggg-3′	This paper	N/A
ALDH7A1 (S102D) primer reverse: 5′-ccccatctccaaagacaccaagtctcctagtacttggatctt-3′	This paper	N/A
LbNOX subclonal primer forward: 5’-ATCGGATCCATGAAGGTCACCGTGG-3’	This paper	N/A
LbNOX subclonal primer reverse: 5’-ATCGCTCGAGCATAGATCCACCAGATCC-3’	This paper	N/A
siRNA #1 for human ALDH7A1: 5′-gcagugagcauguuucuugtt-3′ (sense strand)	Yang et al.[13]	N/A
siRNA #2 for human ALDH7A1: 5′-gcacagcaatggccaaagatt-3′ (sense strand)	Yang et al.[13]	N/A
siRNA for mouse ALDH7A1: 5’-gcagugagcauguuugugatt-3’ (sense strand)	Yang et al.[13]	N/A
siRNA for human ALDH1A1: 5′-gaacaguguggugaauuguu-3′ (sense strand)	Moreb et al.[31]	N/A
siRNA for human ALDH2: 5’-caucucuuaccugguagautt-3’ (sense strand)	Moreb et al.[31]	N/A
siRNA for human ALDH3A1: 5’-gaagaugauugcagagacatt-3’ (sense strand)	Tiedemann et al.[32]	N/A
siRNA for human ALDH5A1: 5’-cggaaguggguacaauuuaatt-3’ (sense strand)	Tiedemann et al.[32]	N/A
siRNA for human AMPKα1: 5′-agugaagguuggcaaacautt-3′ (sense strand)	Yang et al.[33]	N/A
siRNA #1 for human FSP1: 5’-gcaccggcaucaagaucaatt -3’ (sense strand)	Lu et al.[34]	N/A
siRNA #2 for human FSP1: 5’-GCUGCCUCUCAAUGAGUAUTT -3’ (sense strand)	Lu et al.[34]	N/A
siRNA for human ACSL4: 5’-gaggcuuccuaucugauuatt-3’ (sense strand)	Li et al.[35]	N/A
Human ALDH7A1 si resistant primer reverse: 5′-cactgctccaagaaacatcgacactgcctgcttggtgtg-3′	Yang et al.[13]	N/A
Recombinant DNA		
ALDH7A1 in pcDNA3	Yang et al.[13]	N/A
ALDH7A1 in pEGFP-N1	Yang et al.[13]	N/A
ALDH7A1 in pET-15b	Yang et al.[13]	N/A

(*Continued on next page*)

Continued

REAGENT or RESOURCE	SOURCE	IDENTIFIER
LbNox in pcDNA3	This paper	N/A
FSP1 in pET3c-FSP1	This paper	N/A
FSP1 in pEGFP-N1	This paper	N/A
N-myristoyltransferase in pBB131	Yang et al.[13]	N/A
CRISPR/Cas9 KO plasmid	Santa Cruz	sc-417902
Software and algorithms		
GraphPad Prism 9	GraphPad	https://www.graphpad.com
XFe24 Extracellular Flux Analyzer	Seahorse Biosciences	https://www.agilent.com/
Fiji: ImageJ	Fiji	https://fiji.sc/
Other		
GeneJet Plus	SignaGen	SL100499
PepMute	SignaGen	SL100566

EXPERIMENTAL MODEL AND STUDY PARTICIPANT DETAILS

Cells

HeLa, HEK 293 and MEF were obtained from American Type Culture Collection (ATCC). MDA231, MDA436, MDA453, MCF7, H460, and A549 cells were gifts from Joan Brugge (Harvard Medical School, Boston, MA). Synoviocytes and NIH-3T3 cells were gifts from Michael Brenner (Brigham and Women's Hospital and Harvard Medical School, Boston, MA). Cells were cultured in Dulbecco's Modified Eagle Medium (DMEM) with 10% fetal bovine serum and supplemented with glutamine and gentamicin. HT1080, HT1080/ GPX4 KO, HT1080/ GPX4 KO/ FSP1 OE, and H460/ FSP1 KO cells have been described previously.[4,23,24] To generate HT1080/ GPX4 KO/ FSP1 OE/ ALDH7A1 knockout cells, CRISPR-mediated knockout of ALDH7A1 in HT1080/ GPX4 KO/ FSP1 OE cells was performed, using the human antiquitin CRISPR/Cas9 KO plasmid from Santa Cruz (sc-417902) according to manufacturer's instructions. Single cell cloning was then performed to achieve a uniform population of ALDH7A1 KO cells. For cells that require culturing with antioxidant for survival, Liproxstatin-1 (0.2 uM) or Ferrostatin-1 (2 uM) was added to the medium.

Animals

48 hours prior to tumor cell implantation into mice, 1 million cells were plated into a 10 cm dish and cultured in media lacking ferrostatin-1. At the time of injection, all cell lines contained more than 90% viability as assessed via trypan blue staining. For tumor growth studies, 50,000 cells were resuspended in 100 ul of sterile PBS and injected into the dorsal left flank of 6-8 weeks old male NSG mice (n= 3-5 mice per group). Liproxstatin-1 (10 mg/kg) or solvent was administered intraperitoneally daily. Tumor size was measured at least once per week or at the indicated timepoints using a vernier caliper. Estimated tumor volume was determined using the following formula: Tumor volume = length x width^2/2, where length represents the largest tumor diameter and width represents the perpendicular tumor diameter. Twenty-one days after tumor cell implantation, mice were euthanized and dissected tumors were weighed. All animal studies were performed in accordance with guidelines from the institution committee on animal care.

METHOD DETAILS

Chemicals

NAD, NADH, octanal, and hydrogen peroxide were obtained from Sigma. A-769662, AICAR, RSL3, DTUN, Erastin, Liproxstatin-1, Ferrostatin-1, DFO, FINO2, zVAD-FMK, and Necrostatin-1 were obtained from Cayman Chemicals. These chemicals were added for 24 hours in cell death assays, and 2 hours in all other assays that include examination of lipid peroxidation, NADH level, membrane recruitment, and intracellular colocalizations. Cholesterol, sphingomyelin, dioleoyl-phosphatidylcholine (DOPC), dioleoyl-phosphatidylethanolamine (DOPE), dioleoyl-phosphatidylserine (DOPS), dioleoyl-phosphatidylinositol (DOPI), phosphatidic acid (PA), and 1-stearoyl-2-arachidonoyl-sn-glycero-3-phosphoethanolamine (PUFA-PE) were obtained from Avanti Polar Lipids. C11 BODIPY 581/591 was obtained from Invitrogen. Detection kits for NAD/NADH, MDA and 4-HNE were obtained from Sigma.

Antibodies

Antibodies against the following have been described in our previous studies[13,33]: ALDH7A1 (WB 1:1000, IF 1:500), β-actin (WB 1:1000) cellubrevin (Cbv, WB 1:1000), GAPDH (WB 1:1000), Flag epitope (WB 1:1000), HA epitope (WB 1:200), and Myc epitope (WB 1:200). Antibodies against the following were obtained from commercial sources: FSP1 [mouse monoclonal (AMID, WB 1:500) and rabbit polyclonal (WB 1:5000), Santa Cruz], ACSL4 (mouse monoclonal, Santa Cruz, WB 1:100), AMPKα1 (2603S, Cell

signaling, WB 1:500), phospho-substrates of AMPK (5759S, Cell Signaling, WB 1:500), 6xHis epitope (rabbit polyclonal, Santa Cruz, WB 1:1000), GFP (MA5-15256, Thermo Scientific, WB 1:1000), and GST (sc-138, Santa Cruz Biotechnology, WB 1:1000). Mouse anti-calnexin (AF8) was a gift from Michael Brenner (Brigham and Women's Hospital and Harvard Medical School, Boston, MA) and mouse anti-coatomer (CM1A10) was a gift from James Rothman (Yale School of Medicine, New Haven, CT). Conjugated secondary antibodies were obtained from Jackson ImmunoResearch: horseradish peroxidase-conjugated donkey antibodies against mouse IgG (715-03 150, WB 1:10,000) and against rabbit IgG (711-035-152, WB 1:10,000), Cy2 donkey antibodies against mouse IgG (715-225-151, IF 1:200) and against rabbit IgG (711- 225-152, IF 1:200), Cy3 goat antibody against mouse IgG (115-165-062, IF 1:200), Cy3 donkey antibodies against rabbit IgG (711-165-152, IF 1:200) and against sheep IgG (713-165-147, IF 1:200).

Plasmids

ALDH7A1 subcloned into mammalian expression vectors, pcDNA3.1 and pEGFP-N1, have been described previously.[13] Mutant ALDH7A1 (E268Q) was generated using QuikChange Site-Directed-Mutagenesis (Stratagene) with paired oligonucleotides: 5′-gggagaagtctgttgcaacttggaggaaacaatgcc-3′ and 5′-ggcattgtttcctccaagttgcaacagacttctccc-3′. Mutant ALDH7A1 (S102A) was generated with paired oligonucleotides: 5′-aagatccaagtactaggagccttggtgtctttggagatgggg-3′ and 5′-ccccatctccaaagacaccaaggctcctagtacttggatctt-3′. Mutant ALDH7A1 (S102D) was generated with paired oligonucleotides: 5′-aagatccaagtactaggagacttggtgtctttggagatgggg-3′ and 5′-ccccatctccaaagacaccaagtctcctagtacttggatctt-3′. FSP1 and ACSL4 subcloned into mammalian expression vectors have been described previously.[4,21] LbNox was subcloned into the BamH1 and Xho1 sites in pcDNA3.1 by PCR, using primers 5'-ATCG GATCCATGAAGGTCACCGTGG-3' and 5'-ATCGCTCGAGCATAGATCCACCAGATCC-3' and LbNox in pUC57 (obtained from Addgene) as the template to generate a LbNox insert having the appropriate restriction sites.

Purification of recombinant proteins

Recombinant forms of ALDH7A1 have been described previously.[13] Recombinant myristolyated FSP1 was generated by subcloning FSP1 into the pET3c-FSP1 vector. BL21 (DE3) bacteria were then transformed with this construct along with an N-myristoyltransferase construct. Bacteria were then pelleted, lysed, sonicated, followed by centrifugation to obtain the supernatant that contains soluble proteins, which was then applied to a HiTrap Q column. The flow through from this column was then applied to a Superdex 75 pg column. Fractions that contained FSP1 (as tracked by gel staining) were then pooled and applied to a hydrophobic column, HiTrap Phenyl HP. Whereas myristoylated FSP1 binds to this column, the non-myristoylated form does not. The bound protein was then eluted from the column by a NaCl gradient (from 3M to 100 mM), with peak elution occurring at 1.5 M NaCl. Fractions that contained FSP1 (as tracked by gel staining which detected a single band) were pooled and then dialyzed. Aliquots were then snap frozen and stored at -80°C.

Transfection and siRNA

Transfection of DNA plasmids was performed using GenJet Plus (SL100499, SignaGen). Treatment with siRNA was performed using PepMute (SL100566, SignaGen). Plasmid transfections occurred over 48 hours and siRNA transfections occurred over 72 hours. The following siRNA sequences were obtained (Dharmacon) to target: human ALDH7A1, 5′-gcagugagcauguuucuugtt-3′ (sense strand) and 5′-caagaaacaugcuca cugctt-3′ (complement strand), mouse ALDH7A1, 5'-gcagugagcauguuugugatt-3' (sense strand) and 5'-ucacaaacaugcucacugctt-3' (complement strand), human ALDH1A1, 5′-gaacagugugggugaauuguu-3′ (sense strand) and 5′-caauucacccacacuguuc-3′ (complement strand), human ALDH2, 5'-caucucuuaccugguagautt-3' (sense strand) and 5'-aucuaccag guaagagaug-3' (complement strand), human ALDH3A1, 5'-gaagaugauugcagagacatt-3' (sense strand) and 5'-ugucucugcaaucaucuucctt-3' (complement strand), human ALDH5A1, 5'-cggaagugguacaauuuaatt-3' (sense strand) and 5'-uuaaauuguaccacuuccgtt-3' (complement strand), human AMPKα1, 5′-agugaagguuggcaaacautt-3′ (sense strand) and 5′-auguuugccaaccuucacutt-3′ (complement strand), human FSP1, 5'-gcaccggcaucaagaucaatt -3' (sense strand) and 5'-uugaucuugaugccggugctt-3' (complement strand), and human ACSL4, 5'-gaggcuuccuaucugauuatt-3' (sense strand) and 5'-uaaucagauaggaagccuctt-3' (complement strand). Targeting specificities of these siRNAs have been documented previously.[13,35,31–34] Rescue plasmids for wild-type and catalytic dead mutant of human ALDH7A1 were generated by targeting the siRNA sequence using QuikChange Site-Directed-Mutagenesis (Stratagene) with paired oligonucleotides: 5′-cacaccaagcaggcagtgtcgatgtttcttggagcagtg-3′ and 5′-cactgctccaagaaacatcgacactgcctgcttggtgtg-3′.

Subcellular fractionation

To obtain total membranes versus cytosol fractions, cells were washed with PBS, resuspended in homogenization buffer (0.25M sucrose, 1mM EDTA, and 20mM HEPES-KOH, pH 7.4 and protease inhibitor cocktail) and then disrupted by passing through 28-gauge needles. After low-speed centrifugation (800×g for 6 minutes) to pellet nuclei and unbroken cells, the resulting post-nuclear supernatant was centrifuged at 100,000×g for 1 hour to obtain cytosol and total membrane fractions. To obtain mitochondrial versus non-mitochondrial fractions, the Mitochondria Fractionation Kit (Millipore, MIT1000) was used according to manufacturer's instructions.

Membrane treatments

For bicarbonate treatment, 100 ug of membrane was resuspended and incubated in 100 ul of cold 0.1M Na_2CO_3 (pH11.0) for 30 minutes on ice. For treatment with proteinase K, 100 ug of membrane was resuspended in 100 ul of solution and then incubated with

proteinase K (50 ug/ml) at 37°C for 1 hour, followed by incubation at 95°C for 5 minutes to deactivate proteinase K. For KCl treatment, 100ug of membrane was resuspended in 100ul of cold KCl solution that contains 10mM Hepes-KOH, 2.5mM $Mg(OAc)_2$, 200mM Sucrose, pH7.2, and different KCl concentrations for 30 minutes at 4°C. For membrane permeabilization, 0.2% saponin treatment was done at room temperature for 15 minutes.

Frex biosensor measurement

HeLa cells were transfected with siRNA as indicated and then transfected with cyto-Frex, mito-Frex, cyto-YFP, or mito-YFP expression plasmids. Two days later, cells were trypsinized and seeded in a 96-well fluorescence microplate. After 6 h, the medium was changed to FluoroBrite DMEM (Life Technologies), and the fluorescence intensity at 530 nm was measured using excitation wavelengths of 420 nm and 478 nm. The background fluorescence was subtracted and the F478/F420 fluorescence ratio was calculated. The Frex fluorescence ratios were divided by the YFP fluorescence ratios to correct for pH-dependent effects on biosensor intensity.

Extracellular flux measurement

Oxygen consumption rate (OCR) and extracellular acidification rate (ECAR; a surrogate for lactate production) were measured using an XFe24 Extracellular Flux Analyzer (Seahorse Biosciences). HeLa cells transfected with siRNA as indicated. Cells were seeded at a density of 25,000 cells per well 24 hour prior to the assay. For mitochondrial stress assays, oligomycin (1 μM), FCCP (0.5 μM) and antimycin A/rotenone (0.5 μM each) were added to determine the OCR for ATP synthesis, the maximal OCR, and OCR independent of electron transport, respectively. For glycolysis stress assays, glucose (10 mM), oligomycin (1 μM), and 2-deoxyglucose (50 mM) were added to determine glycolytic flux and glycolytic capacity. At the conclusion of the assay, cells were stained with CyQuant Direct (Life Technologies) to permit normalization of OCR and ECAR measurements by cell number.

Lipid peroxidation measurement

C11 BODIPY 581/591 was added to cells (final concentration 5 uM) and then incubated at 37°C for 5 minutes. Confocal microscopy was then performed to detect the C11-ox form (green) and the C11-non-ox form (red). 10 images were randomly chosen and then calculated for the color intensity using Image J, with values expressed as C11-ox/(C11-ox+C11-non-ox).

Ubiquinone/ubiquinol measurement

These coenzyme Q10 (CoQ10) forms were measured using UHPLC coupled electrospray ionization tandem mass spectrometry, adapting from previously established method 35. In brief, samples were extracted using 1- propanol containing butylhydroxytoluene as an antioxidant with glass bead homogenization and addition of deuterated oxidized coenzyme Q10 (CoQ10-d10) as an internal standard. After centrifugation, supernatants were analyzed using AB Sciex 4000 or 6500 Q-Trap instruments coupled with Exion or Shimadzu UHPLC systems. Chromatography was carried out with a C8 reverse-phase column (Waters ACQUITY UPLC BEH C8, 2.1 X 50 mm, 1.7 μm) maintained at 40°C. Samples were loaded in water and isocratic elution was performed using 100% methanol containing 5 mM ammonium formate at a flow rate of 0.4 mL/min. We monitored the following precursor/product ion pairs for the indicated analytes: m/z 881/197.1 (UN10, DP 90V, CE 36V), m/z 882.8/197.1 (UL10, DP 115V, CE 54V), and m/z 890/206 (Oxidized CoQ10-d10, IS, DP 95V, CE 35V) with a dwell time of 0.15 s. Quantification was accomplished using multipoint calibration curves for the oxidized and reduced CoQ10 using bovine serum albumin as the matrix and data were reported as ratios of oxidized to reduced CoQ10).

Protein interaction assays

To assess direct interaction through the pulldown approach, GST-ALDH7A1 on glutathione beads were incubated with FSP1-6xHis (100 nM) at 4°C for 1 hour in incubation buffer (PBS with 0.05% Triton X-100 and protease inhibitors). Beads were then collected by centrifugation at 800xg for 5 minutes at 4°C, followed by two times washes with incubation buffer. Samples were then analyzed by immunoblotting for 6xHis and GST. To assess interaction in cells through the co-precipitation approach, cells that express GFP-FSP1 were disrupted in lysis buffer (PBS with 0.5% Triton X-100 and protease inhibitors) at 4°C for 30 minutes. Lysates were then centrifuged at 13,000xg for 20 minutes at 4°C. The supernatant was then incubated with protein A/G PLUS-Agarose beads (sc-2003, Santa Cruz), which was pre-incubated with the anti-GFP antibody for 1 hour at 4°C. Samples were then analyzed by immunoblotting for ALDH7A1 and GFP.

In vitro kinase assay

Purified AMPK (0.1 μg, Promega) was incubated with recombinant ALDH7A1 or FSP1 (10 μg) in 50 μl reaction buffer (25 mM MOPS, pH 7.2, 12.5 mM β-glycero-phosphate, 25 mM $MgCl_2$, 5 mM EGTA, 2 mM EDTA, 0.25 mM DTT, 100 μM AMP, 25 μM ATP and 25 μM ^{32}P-ATP) at 30°C for 30 minutes. Samples were then analyzed by SDS-PAGE followed by autoradiography.

Colocalization studies

Colocalization studies were performed using the Zeiss system equipped with the Zeiss Axio Observer Z1 Inverted Microscope having a Plan-Apochromat 63× objective, the Zeiss LSM 800 with Airyscan confocal package with Zeiss URGB (488 and 561 nm) laser lines, and Zen 2.3 blue edition confocal acquisition software. For quantitation of colocalization, ten fields of cells were examined with each

field typically containing five cells. Images were imported into the NIH Image J version 1.50e software, and then analyzed through a plugin software (https://imagej.Net/Coloc_2). Under the ''Image'' tab, the ''Split Channels'' option was selected. Under the ''Plugins'' tab, ''Colocalization Analysis'' option was selected, and within this option, the ''Colocalization Threshold'' option was selected. Colocalization values were then calculated by the software.

Reconstitution of ALDH7A1 and FSP1 activities

Liposomes were generated from pure defined lipids, with major lipids mimicking the composition of native membrane (mol%): DOPC 50%, DOPE 10%, DOPS 5%, PA 5%, cholesterol 17%, sphingomyelin 7%, PUFA-PE 2% and ubiquinone 4%. These pure lipids were mixed in a glass tube, dried under nitrogen, and then resuspended in PBS, which involved ten times of rapid freeze and thaw with occasional vortexing. To reconstitute ALDH7A1 activity, liposome (1 ug/ul) were incubated with NAD (1 mM), octanol (10 mM), and ALDH7A1 (1 uM) in 200 ul PBS for 1 hour at 37°C. To reconstitute FSP1 activity, FSP1 (1 uM) was added to the ALDH7A1 incubation for 40 minutes. NADH level was measured by detecting OD at 340 nm using Genesys 180 UV-Visible Spectrophotometer (Thermo Scientific).

Reconstitution of lipid peroxidation

To induce lipid peroxidation, 5% hydrogen peroxide or 50 uM of DTUN was added to liposomes. Lipid peroxidation was then detected as described above in using the C11 BODIPY 581/591 biosensor. To assess protection against lipid peroxidation, ALDH7A1 and NAD were added for 10 minutes, and FSP1 was then added for 40 minutes.

Other assays

Cellular ATP level was measured using ATPlite Luminescence Detection Assay System (Perkin Elmer) with final values normalized to the number of viable cells. Cell viability was typically assessed by trypan-blue staining. The PrestoBlue Cell viability reagent (Invitrogen, A13261) was used in Figures S2A and S2C to confirm the results of trypan-blue staining, with quantitation obtained by measuring absorbance at 570 nm wavelength. NAD/NADH measurements were performed using a standard enzyme cycling assay, which involved a NAD/NADH Kit (MAK037, Sigma) with quantitation obtained by measuring absorbance at 450 nm wavelength. NADPH measurements were performed also by an enzyme cycling assay, which involved a NADPH Kit (MAK038, Sigma) with quantitation obtained by measuring absorbance at 450 nm. MDA measurements were done using an assay kit (MAK 085, Sigma) that produces a colorimetric product with quantitation obtained by measuring absorbance at 532 nm wavelength. 4-HNE measurements were done using an assay kit (ab238538, Abcam) with quantitation obtained by measuring absorbance at 450nm. For all assays, controls were included to detect background levels for normalization of experimental values.

QUANTIFICATION AND STATISTICAL ANALYSIS

Sample sizes are indicated in the figure legends. Sample size used was based on our previous familiarity with the assays. For comparison between two conditions, significance was tested by the paired two-tailed Student's t-test. For comparison among multiple conditions, significance was tested by the analysis of variance (ANOVA). These tests were performed using Excel or Prism software. We used standard techniques for which no inclusion/exclusion criteria were pre-established. The experiments were not randomized. The investigators were not blinded to the group allocation during experiments and in outcome assessment.

Supplemental figures

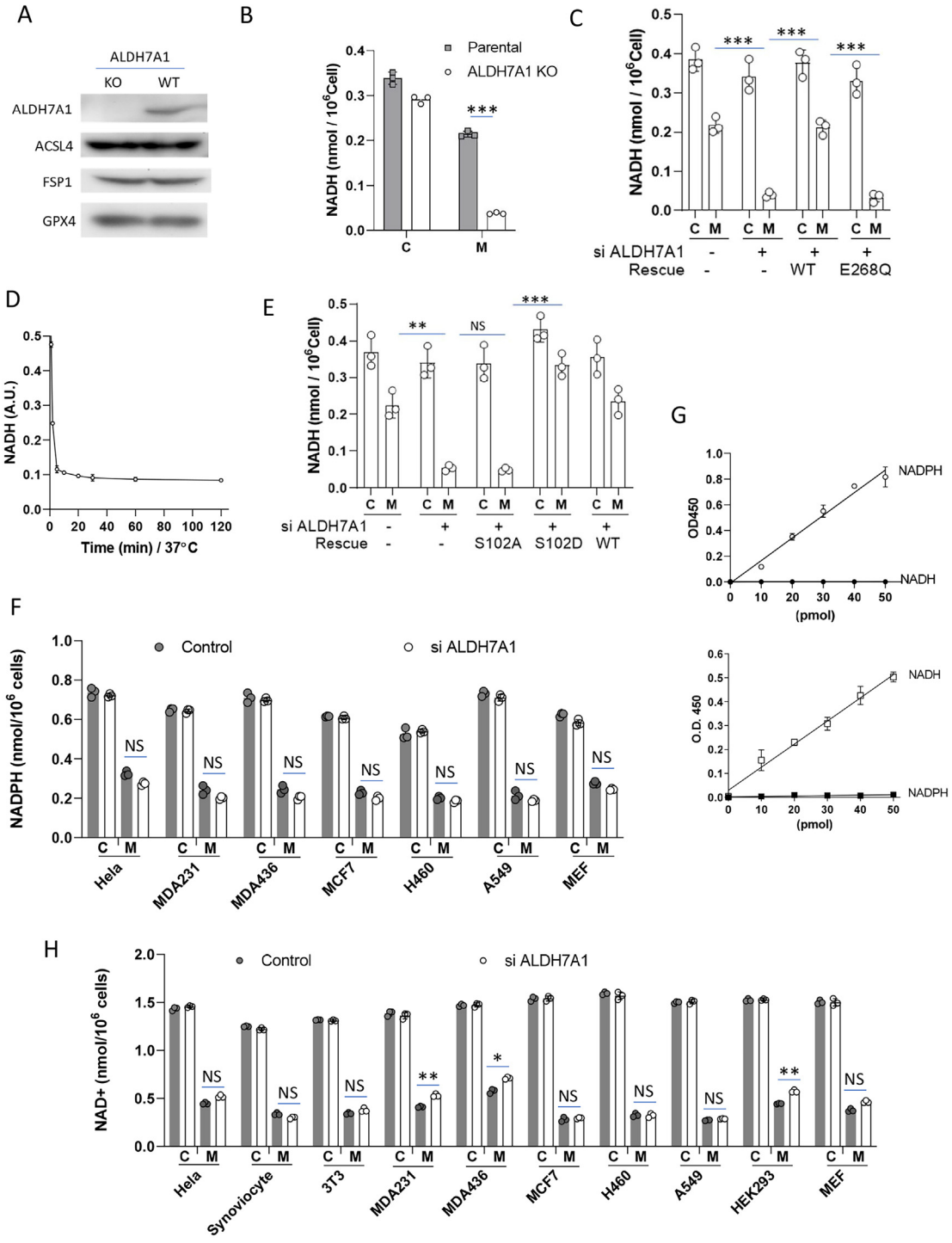

Figure S1. Further characterizing membrane NADH generated by ALDH7A1, related to Figure 2

(A) Confirmation of ALDH7A1 KO in HeLa cells by CRISPR-Cas9, *n* = 2.

(B and C) NADH level in total membranes and cytosol from HeLa cells that were treated as indicated, *n* = 3.

(D) Time course of NADH level in the lipid-bound fraction of total membranes upon incubation with buffer, *n* = 2.

(legend continued on next page)

(E) NADH level in total membranes and cytosol from HeLa cells that express ALDH7A1 forms as indicated, $n = 3$.
(F) NADPH level in total membranes and cytosol from HeLa cells that were treated as indicated, $n = 3$.
(G) Confirming the specificity of detecting NADH versus NADPH by assessing samples with increasing levels of both compounds, $n = 2$.
(H) NAD level in total membranes and cytosol from HeLa cells that were treated as indicated, $n = 3$.
Quantitative data are shown as mean ± SD; ***$p < 0.0005$, **$p < 0.005$, *$p < 0.05$, NS $p > 0.05$, Student's t test.

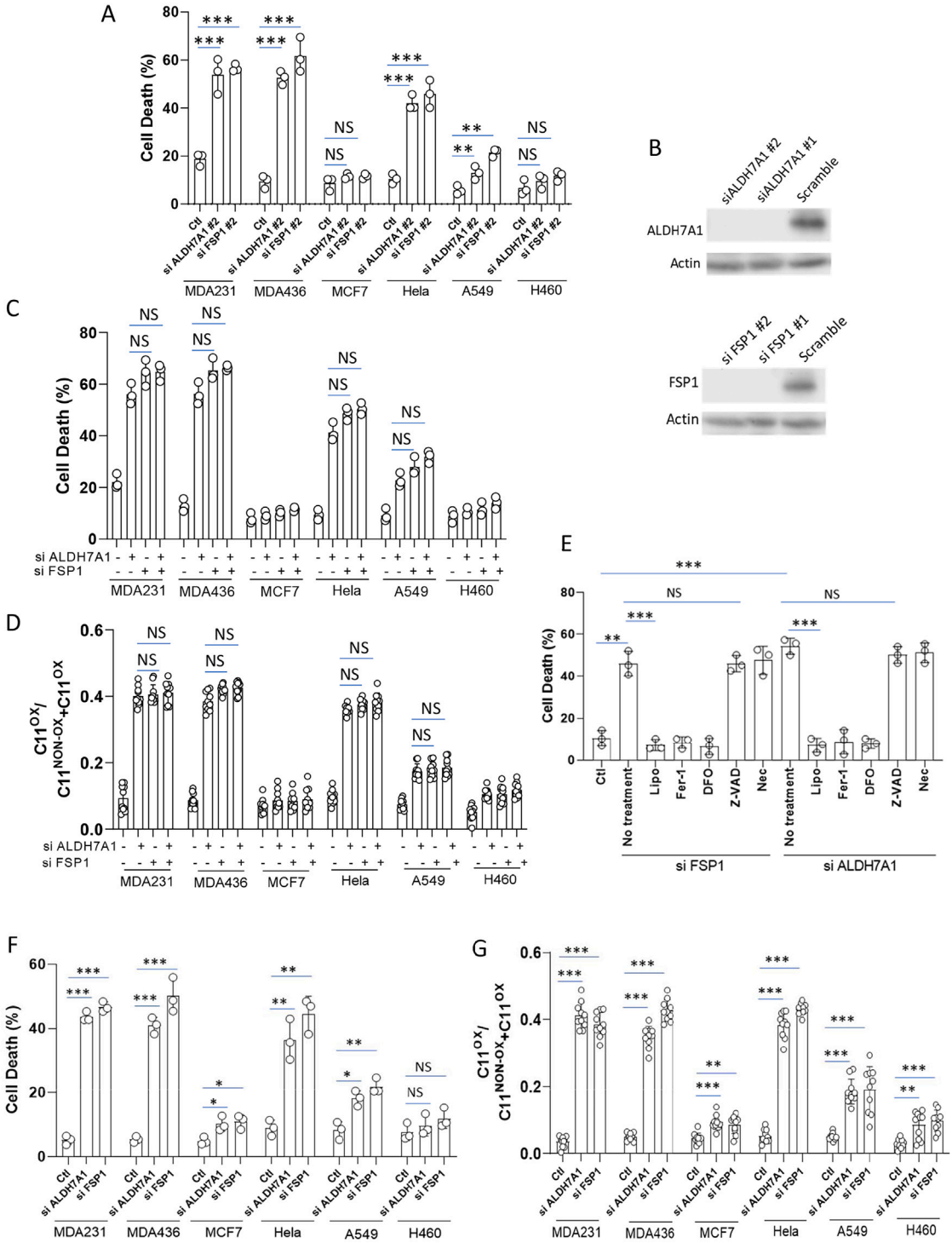

Figure S2. Further characterizing ferroptosis protection by ALDH7A1, related to Figure 3

(A) Quantitation of cell death upon treatment with RSL3 (100 nM) and a second set of siRNAs against targets as indicated, *n* = 3.

(B) Confirming the efficacy of siRNA treatments, *n* = 2.

(C) Quantitation of cell death upon treatment with RSL3 (100 nM) and siRNA as indicated, *n* = 3.

(D) Quantitation of lipid peroxidation upon treatment with RSL3 (100 nM) and siRNA as indicated, *n* = 3. A representative experiment is shown.

(legend continued on next page)

(E) Cell death was quantified for MDA231 cells treated with RSL3 (100 nM) along with siRNA and chemical inhibitors as indicated, $n = 3$.
(F) Cell death was quantified for cells treated with erastin (2 μM) and siRNA as indicated, $n = 3$.
(G) Quantitation of lipid peroxidation upon treatment with erastin (2 μM) and siRNA as indicated, $n = 3$. A representative experiment is shown.
Quantitative data are shown as mean ± SD; ***$p < 0.0005$, **$p < 0.005$, *$p < 0.05$, NS $p > 0.05$, Student's t test.

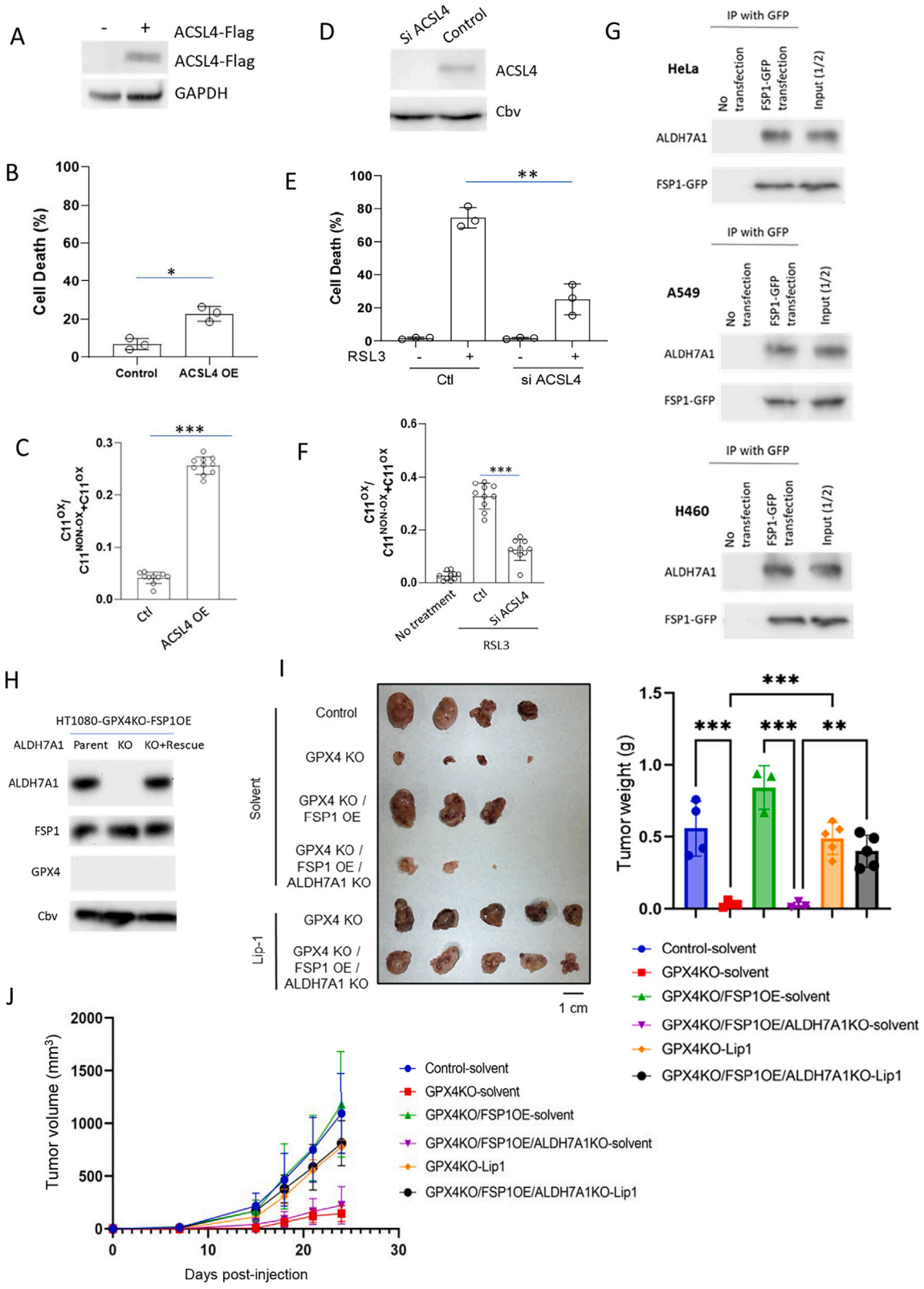

(legend on next page)

Figure S3. Further characterizing how ALDH7A1 protects against ferroptosis, related to Figure 3

(A) Immunoblotting confirming the expression of transfected flag-tagged ACSL4 in MCF7 cells, $n = 2$.

(B) Cell death was quantified for MCF7 cells treated with RSL3 (100 nM) and transfection as indicated, $n = 3$.

(C) Lipid peroxidation was quantified for MCF7 cells treated with RSL3 (100 nM) and transfection as indicated, $n = 3$. A representative experiment is shown.

(D) Immunoblotting confirming the efficacy of siRNA against ACSL4 in MDA231 cells, $n = 2$.

(E) Cell death was quantified for MDA231 cells treated as indicated, RSL3 (1 μM), $n = 3$.

(F) Lipid peroxidation was quantified for MDA231 cells treated as indicated, RSL3 (1 μM), $n = 3$. A representative experiment is shown.

(G) Interaction between endogenous ALDH7A1 and transfected GFP-tagged FSP1 in different cells as assessed by a co-precipitation experiment, $n = 2$.

(H) Immunoblotting confirming the efficacy of ALDH7A1 KO and rescue, $n = 2$.

(I) Tumor growth in mice that had been implanted with different HT1080 cells as indicated. Shown are primary images of excised tumors 24 days after implantation as well as quantitation (control: $n = 4$, GPX4 KO: $n = 4$, GPX4 KO/FSP1 OE: $n = 3$, GPX4 KO/FSP1 OE/ALDH7A1 KO: $n = 3$, GPX4 KO-Lip1: $n = 5$, GPX4 KO/FSP1 OE/ALDH7A1 KO/Lip1: $n = 5$), $^{**}p < 0.01$, $^{***}p < 0.001$, one-way ANOVA followed by Tukey's post hoc test.

(J) Kinetics of tumor growth in mice implanted with different HT1080 cells as indicated, $n = 2$.

Quantitative data are shown as mean ± SD; $^{***}p < 0.0005$, $^{**}p < 0.005$, $^{*}p < 0.05$, Student's t test (unless otherwise indicated).

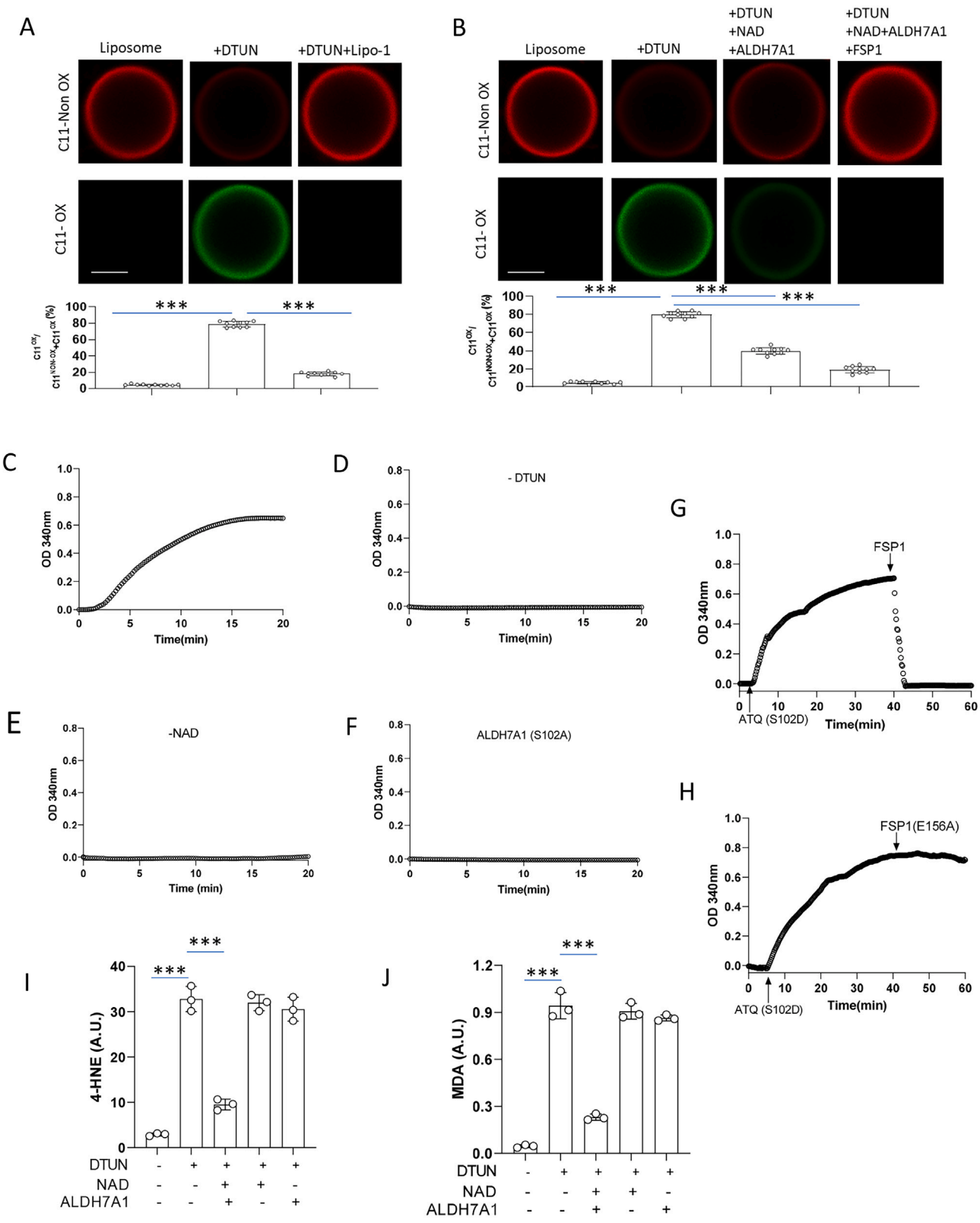

(legend on next page)

Figure S4. Reconstituting protection by ALDH7A1 and FSP1 against lipid peroxidation induced by DTUN, related to Figure 4

(A and B) Lipid peroxidation of liposomes in different conditions as indicated, as assessed by confocal microscopy detecting the biosensor, $n = 3$. A representative experiment is shown having primary images, bar: 10 μm, and quantitation.

(C–F) NADH level, as tracked by OD at 340 nm, was quantified, comparing when ALDH7A1 activity was reconstituted (by incubating liposomes subjected to hydrogen peroxide with NAD and ALDH7A1) versus conditions when different components are omitted or when mutant ALDH7A1 was used, $n = 3$.

(G and H) NADH level, as tracked by OD at 340 nm, was quantified, examining the effect of FSP1 form as indicated being added to liposomes for which ALDH7A1 activity had been reconstituted, $n = 3$.

(I and J) 4-HNE (I) or MDA (J) level was quantified upon the incubation of liposomes with different components as indicated, $n = 3$.

Quantitative data are shown as mean ± SD; $^{***}p < 0.0005$, Student's t test.

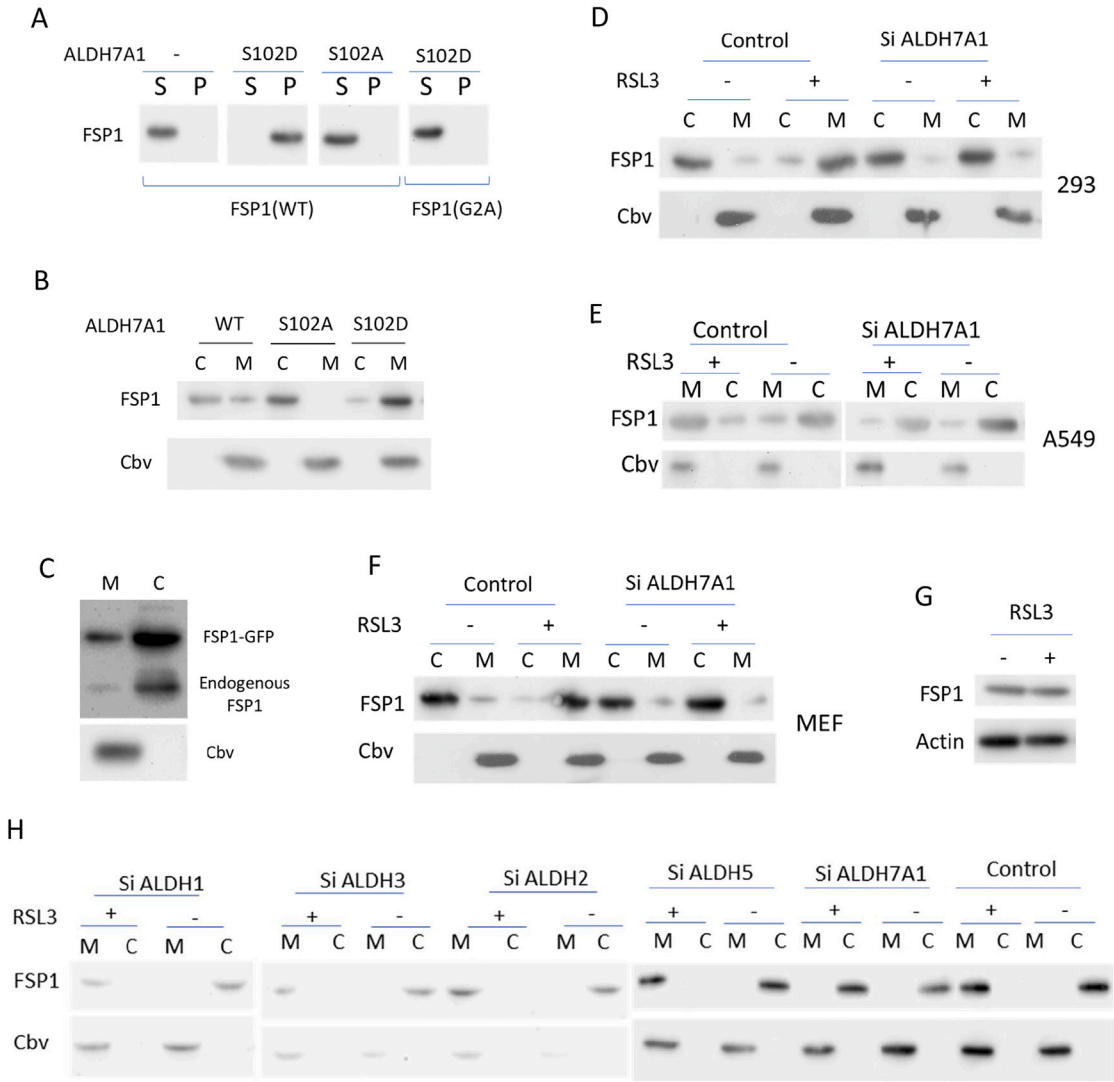

Figure S5. Further characterizing how ALDH7A1 recruits FSP1 to membranes, related to Figure 6

(A) FSP1 level on the membrane and in the supernatant upon the incubation of FSP1 (WT having myristoylation, G2A not having myristoylation) with liposomes and ALDH7A1 form as indicated, $n = 2$.

(B) FSP1 and Cbv levels on total membranes and in cytosol from MDA231 cells that express ALDH7A1 forms as indicated, $n = 2$.

(C) Total FSP1 expression level, comparing MDA231 cells that were untransfected or transfected with FSP1-GFP, $n = 2$.

(D–F) FSP1 and Cbv levels on total membranes and in cytosol from different cells that were treated with RSL3 (100 nM) and/or siRNA as indicated, $n = 2$.

(G) Immunoblotting confirming RSL3 (100 nM) treatment of MDA231 cells acutely (2 h) does not affect FSP1 expression level, $n = 2$.

(H) FSP1 and Cbv levels on total membranes and in cytosol from MDA231 cells that were treated with RSL3 (100 nM) and/or siRNA as indicated, $n = 2$.

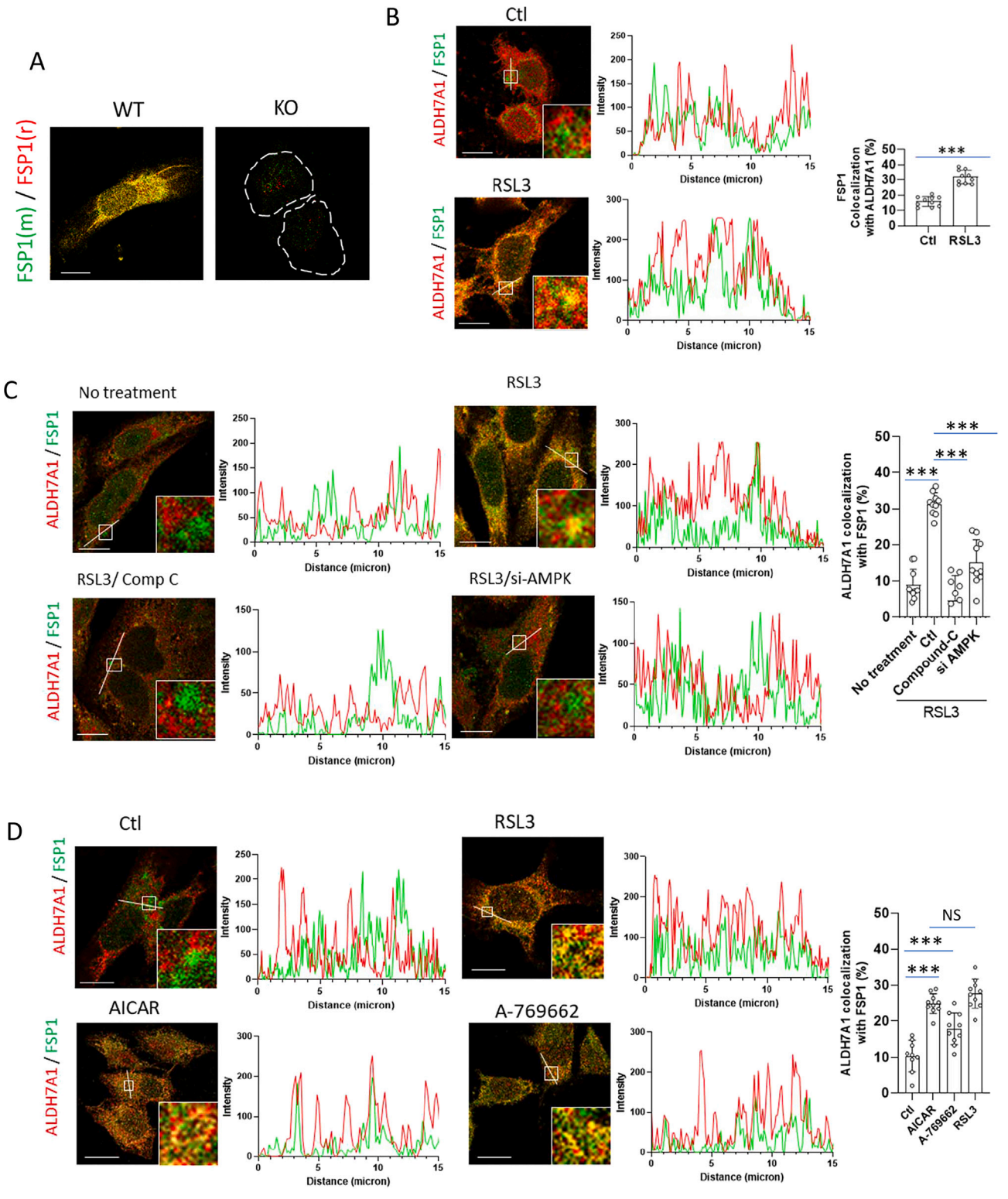

(legend on next page)

Figure S6. Characterizing how ferroptotic stress induces the colocalization of ALDH7A1 and FSP1, related to Figure 6

(A) Confirming the specificity of a mouse (green) or a rabbit (red) antibody against FSP1 by comparing immune staining of H460 cell, WT or KO, $n = 2$.

(B–D) Colocalization of ALDH7A1 and FSP1, as assessed by confocal microscopy examining MDA231 cells treated as indicated, RSL3 (100 nM), $n = 2$. A representative experiment is shown with primary images, ALDH7A1 (red) and FSP1 (green), bar: 10 μm, line scans quantifying the fluorescence intensities, and quantitation.

Quantitative data are shown as mean ± SD; $^{***}p < 0.0005$, $^{*}p < 0.05$, Student's t test.

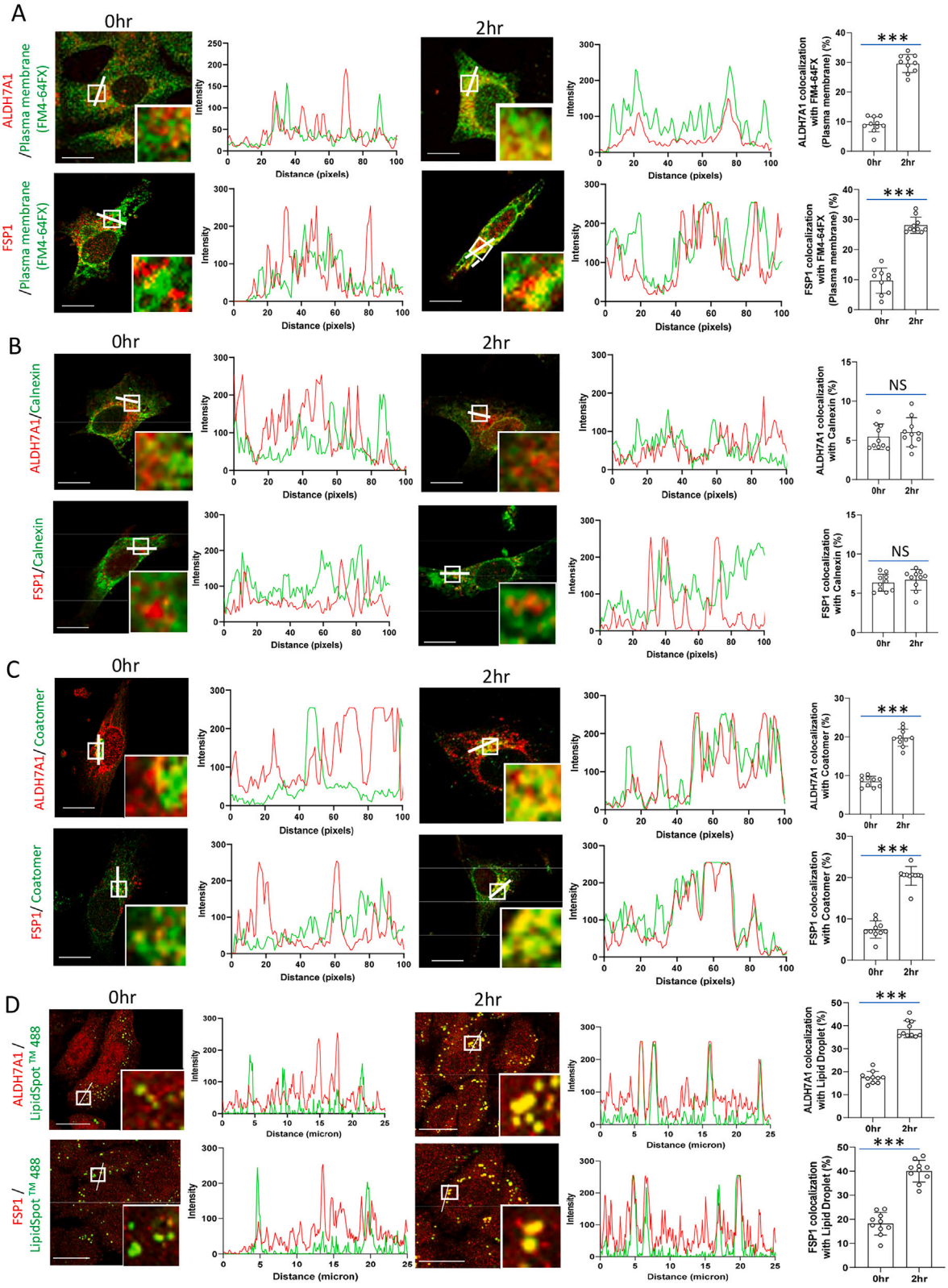

(legend on next page)

Figure S7. Identifying membrane compartments to which ALDH7A1 and FSP1 are recruited, related to Figure 6

(A–D) Colocalization of ALDH7A1 and FSP1 with organelle markers upon treatment of MDA231 cells with RSL3 (100 nM) for times indicated, as assessed by confocal microscopy, $n = 2$. A representative experiment is shown with primary images, bar: 10 μm, line scans quantifying the fluorescence intensities, and quantitation. (A) ALDH7A1 (red) and a plasma membrane marker (FM4-64FX incubated with cells at 4°C, green), (B) ALDH7A1 (red) and ER marker (calnexin, green), (C) ALDH7A1 (red) and Golgi marker (coatomer, green), and (D) ALDH7A1 (red) and lipid droplet marker (LipidSpot 488, green).